THE PENNSYLVANIA STATE UNIVERSITY
SCHREYER HONORS COLLEGE

DEPARTMENT OF MECHANICAL ENGINEERING

SIMULATION OF SWIRLING FLOW THROUGH NOZZLES FOR A BIDIRECTIONAL VORTEX ROCKET ENGINE

ROHAN GAGLANI
SPRING 2017

A thesis
submitted in partial fulfillment
of the requirements
for a baccalaureate degree
in Mechanical Engineering
with honors in Mechanical Engineering

Reviewed and approved* by the following:

Brian Maicke
Associate Professor of Mechanical Engineering; Science, Engineering, and Technology
Thesis Supervisor

Ronald Walker
Associate Professor of Mathematical Sciences; Science, Engineering, and Technology
Honors Adviser

* Signatures are on file in the Schreyer Honors College.

ABSTRACT

The purpose of this research is to simulate the swirling flow through a nozzle, which would be attached to the exhaust of the bidirectional vortex rocket nozzle. The simulation is conducted using a simulation software called STAR CCM+, a computational fluid dynamics program. In this numerical analysis, information is collected regarding the influence of swirling flow on the shock structure and Mach number of the nozzles. Two different nozzle geometries (conical and parabolic) are used for the simulation and the results are compared to simulations without swirling flow. The study is used to verify previous theoretical and experimental results and also to verify nozzle geometries proposed for the bidirectional vortex rocket engine design at Penn State Harrisburg. The simulations for the most part shows agreement with the experimental and theoretical results in terms of the effect of swirl on the shock structures and locations. While the shock structure is largely unchanged in the presence of swirl for the conical nozzle, a change in shock location is noticed in the parabolic nozzle case, which can be an important area of interest for further research. The study also examines the mass flow rates for the two types of flows and shows a reduction in the mass flow rate for the nozzle with swirling flow in the case of a conical nozzle.

TABLE OF CONTENTS

LIST OF FIGURES iii

LIST OF TABLES iv

ACKNOWLEDGEMENTS v

Chapter 1 Introduction and Literature Review 1

- Historic Overview 1
- The Bidirectional Vortex Rocket Engine 3
- Rocket Nozzles 5
  - Nozzle Area (Expansion) Ratio 6
  - Types of Nozzles 7
- Conclusion 12

Chapter 2 14

- Research Purpose 14
- Research Design 14
  - Geometry 14
  - Meshing 18
  - Physics and Setup 20

Chapter 3 Star CCM+ Simulation for Conical Nozzles 23

- Residuals 24
- Mach Number 26
  - Mach Number Contour 26
  - Mach Number Scatter 28
- Pressure 29
  - Pressure Plots 29
  - Pressure Scatter 31
- Density 33
- Mass Flow Rate at Outlet 34

Chapter 4 36

- Residuals 36
- Mach Number 38
  - Mach Number Contour 38
  - Mach Number Scatter 39

Pressure 40
Pressure Plots 40
Pressure Scatter 42
Density 44
Mass Flow Rate at Outlet 45

Chapter 5 Conclusion 47

Appendix A Rocket Combustion Chamber and Nozzle Dimensions 49

REFERENCES 51

LIST OF FIGURES

Figure 1. Crack in Combustion Chamber Liner Wall Due to Thermal Ratcheting [4] 2

Figure 2. An Illustration of the Difference between a Traditional Rocket Engine and Bidirectional Vortex Rocket Engine [9] 5

Figure 3. A de Laval Nozzle with its terminology [10] 6

Figure 4. A Conical Nozzle 8

Figure 5. Bell Nozzle Contour [6] 10

Figure 6. Comparison between Conical and Bell Nozzles [6] 10

Figure 7. Parabolic Approximation of a Bell Nozzle [6] 11

Figure 8. The Computational Domain with the External Boundaries Highlighted 16

Figure 9. The Computational Domain with Highlighted Boat Tail and Body of the Nozzle 17

Figure 10. Computational Domain with Highlighted Nozzle Surfaces 1, 2 and 3 17

Figure 11. Polyhedral Mesh Generated in Star CCM+ for a Conical Nozzle 19

Figure 12. Polyhedral Mesh Generated in Star CCM+ for a Parabolic Nozzle 20

Figure 13. Residuals No-Swirl 24

Figure 14. Residuals Swirl 25

Figure 15. Mach Number Contours of Non-Swirling Fluid 26

Figure 16. Mach Number Contours of Swirling Fluid 27

Figure 17. Mach Number Values(scatter) with Respect to the x Axis for Non-Swirling Fluid. 28

Figure 18. Mach number Values(scatter) with Respect to the x Axis for Swirling Fluid. 28

Figure 19. Pressure at the Centerline of the Nozzle 29

Figure 20. Pressure at the Wall of the Nozzle 30

Figure 21. Pressure Along the Symmetry Axis of the Nozzle Body 30

Figure 22. A Scatter Chart for the Various Pressure Values for Non-Swirling Flow .31

Figure 23. A Scatter Chart for the Various Pressure Values for Swirling Flow.....32

Figure 24. Density Contours of Non-Swirling Fluid 33

Figure 25. Density Contours of Swirling Fluid 33

Figure 26. Average Mass Flow Rate at Outlet for Non-Swirling Fluid.....34

Figure 27. Average Mass Flow Rate at Outlet for Swirling Fluid.....35

Figure 28. Residuals No-Swirl.....36

Figure 29. Residuals Swirl.....37

Figure 30. Mach Number Contours of Non-Swirling Fluid 38

Figure 31. Mach Number Contours of Swirling Fluid.....38

Figure 32. Mach Number Values(scatter) with Respect to the x Axis for Non-Swirling Fluid. 39

Figure 33. Mach Number Values(scatter) with Respect to the x Axis for Swirling Fluid.39

Figure 34. Pressure at the Centerline on the Nozzle.....40

Figure 35. Pressure at the Wall of the Nozzle 41

Figure 36. Pressure Along the Symmetry Axis of the Body.....41

Figure 37. A Scatter Chart for the Various Pressure Values for Non-Swirling Flow .42

Figure 38. A Scatter Chart for the Various Pressure Values for Swirling Flow.....43

Figure 39. Density Contours of Non-Swirling Fluid 44

Figure 40. Density Contours of Swirling Fluid 44

Figure 41. Average Mass Flow Rate at the Outlet for Non-Swirling Fluid.....45

Figure 42. Average Mass Flow Rate at the Outlet for Swirling Fluid.....45

ACKNOWLEDGEMENTS

I would like to thank my advisor Professor Maicke for all his help and support through the research. Professor Maicke introduced me to the topic in Summer of 2016 for an REU project and I enjoyed working with him on the project ever since. I have enjoyed taking his aerospace engineering related course throughout my undergraduate studies

I would also like to thank Professor Abu Ayyad who in spite of his busy schedule took the time out to help me with the research.

I thank Professor Ronald Walker who introduced me to and got me interested to the Honors Program. Without his through recruiting efforts and continuous support, this research would not have been possible.

Special thanks to fellow researcher Gerardo Talamantes for his expertise in the field of the bidirectional vortex rocket engine, and his constant will to help me with my research.

Finally, I am grateful to Penn State Harrisburg for the resources dedicated towards this research.

Chapter 1

Introduction and Literature Review

Historic Overview

The first ever space launch took place in the July of 1950 with the launch of the first rocket from Cape Canaveral, Fla: The Bumper 2. Bumper 2 was a two-stage rocket that had a V-2 missile base with a Corporal Rocket which was capable of going about 250 miles high. These rockets could carry very small payloads thus allowing them to measure very few attributes. This rocket was launched under the guidance of the General Electric Company. This rocket was primarily used for research on the upper atmosphere of earth. Since then, many advancements have been made in the field of rocket propulsion [1].

In July 2011, NASA declared the retirement of the Space Shuttle Program, it's most advanced and optimized space program till date. By 2011, the three remaining space shuttles, Atlantis, Discovery and Endeavour retired after 33, 39 and 25 missions respectively even though they were designed for a 100 missions each [2]. There are many reasons for the declining interest in the space program and also for the early retirement of NASA's Space Shuttle Program. One of the biggest and most prominent being the expense of sending each of these shuttles to space. According to NASA, the cost of launching one space shuttle in 2011 was $450 million with the average cost per launch being $1.2 billion per launch over the lifetime of the space shuttle program [3]. The cost of the space programs combined with its inefficiencies and uncertainties clearly shows the need for advancement in the field of space rockets.

The Space Shuttle Main Engine (SSME) was, in fact, the first engine designed to be reusable. This engine was meant to withstand very high temperatures that would be produced during combustion. However, the actual life of the Main Combustion Chamber (MCC) is considerably less than the original design life due to cracks which form in the MCC liner wall. The cracks were caused by a plastic strain that was induced due to the high temperatures experienced by the chamber causing the wall between the hot gas and the coolant to get thinner and thinner with each use and thermal cycle. This phenomenon is known as thermal ratcheting, and after numerous thermal cycles, cracks develop as shown in Figure 1 [4].

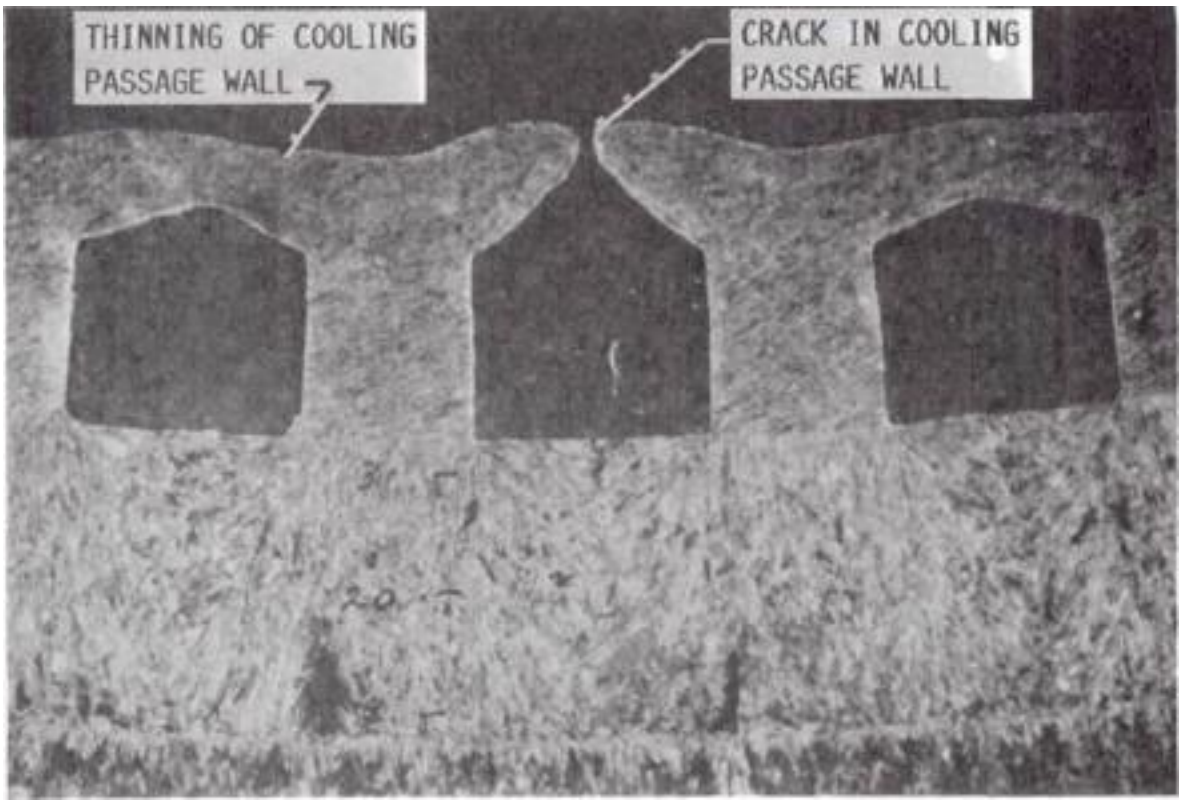

Figure 1. Crack in Combustion Chamber Liner Wall Due to Thermal Ratcheting [4]

The Bidirectional Vortex Rocket Engine

One of the principle goals of aerospace engineering research is to reduce the cost of access to space. To reach this aim, a number of different technologies are being investigated, one of which is the bidirectional vortex rocket engine. This design concept uses swirling oxidizer injection to protect combustion chamber walls from high-temperature combustion products, allowing for the use of thinner, less expensive materials to construct the motor. While the bidirectional vortex has been flown as a technology demonstrator, it has yet to be used at a large scale [5]. The research proposed in this study will add to our existing knowledge on swirl-driven rocket motors and assess the effect of swirl on nozzle performance.

The bidirectional vortex rocket engine presents an improved model of the existing rocket engines showing improvement in the core design requirements of a rocket engine.

The basic design parameters for a rocket engine are [6]-

1. Thrust level
2. Performance (specific impulse)
3. Run duration
4. Propellant mixture ratio
5. Weight of engine system at burnout
6. Envelope (size)
7. Reliability
8. Cost
9. Availability (time table-schedule)

Considering the fact that 51% of the rockets weight is due to the lining of the material to counter the high temperatures and pressures in the combustion chamber, one strategy to increase the efficiency and thus reduce the cost of these engines is to reduce the impact of the temperature on the walls of the engine. The bidirectional vortex rocket engine is a great technological feat that can be used for this purpose [7]. According to Orbitec, the company that was responsible for testing the bidirectional vortex rocket engine, "Orbitec's test engine demonstrated a wall temperature of only 60°C while containing 3000°C combustion in the central vortex. Such a dramatic temperature difference enabled the engine to be built with a 25mm thick Perspex wall; surely the first time anyone has been able to view the inside of a running liquid rocket engine [5]."

Building on the simulation of the bidirectional vortex rocket engine is done Talamantes [8], this research focuses on the simulation of swirling flow of the engine outlet fluid through de-Laval converging-diverging nozzles. The difference between a traditional liquid engine and a vortex rocket engine is illustrated in Figure 2.

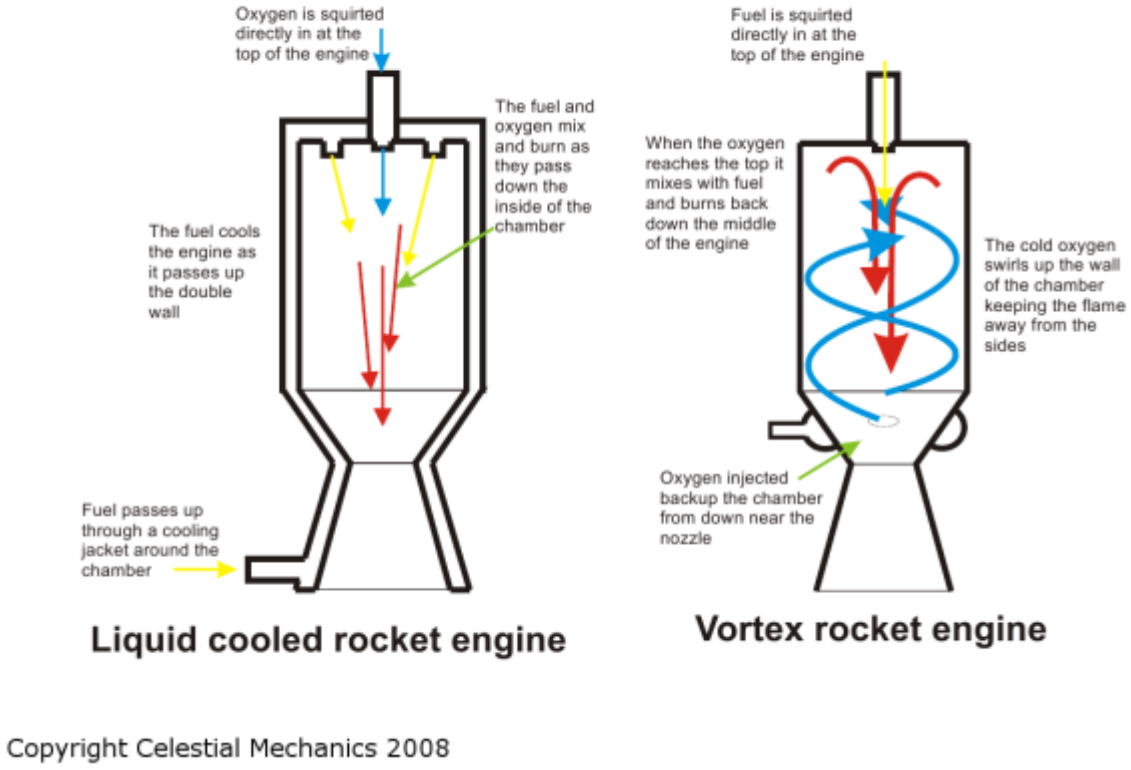

Figure 2. An Illustration of the Difference between a Traditional Rocket Engine and Bidirectional Vortex Rocket Engine [9]

Rocket Nozzles

A nozzle is a device used in different aeronautical and aerospace applications to expand and accelerate the air at the outlet of a combustion chamber. Simply put, a nozzle converts the high pressure inside the combustion chamber of a rocket engine to rapidly moving gas at ambient pressure. There are many types of nozzles, with the de Laval being the most common in propulsion applications. A de Laval nozzle as shown in Figure 3 is an axisymmetric tube pinched in the middle to form a throat. A de Laval nozzle flow chokes at the throat where the cross-sectional area is at its lowest and the velocity at this point will be equal to the speed of sound (Mach 1) at that point,

then as the area increases the velocity of the gas increases with decreasing pressure as the Mach number becomes greater than one after the throat [9].

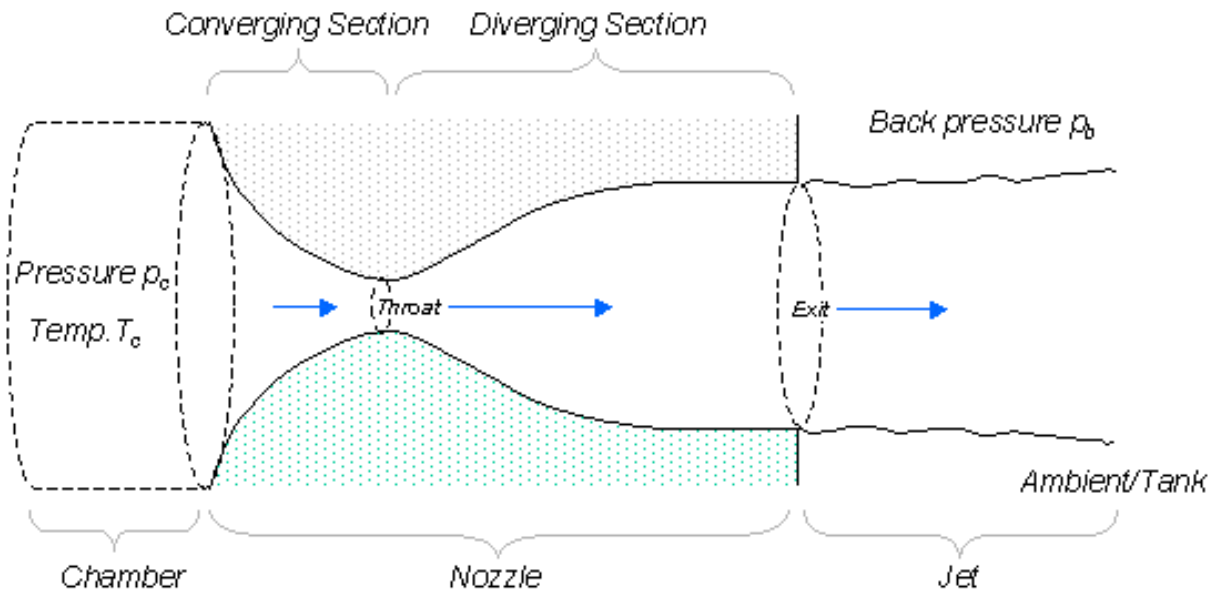

Figure 1. *Converging Diverging Nozzle Configuration*

Figure 3. A de Laval Nozzle with its terminology [10]

Nozzle Area (Expansion) Ratio

With all other parameters fixed, for a particular ratio of chamber pressure to the outside pressure, there is only one area (expansion) ratio of the nozzle which gives the optimal performance. The area ratio of a nozzle also known as the expansion ratio is the ratio of the area of the throat of the nozzle to the outlet of the nozzle. Since the main aim of rockets is to lift vehicles to altitudes, the external pressure may vary from atmospheric to total vacuum. Thus, designers take into account the trajectory of the rocket to ultimately determine the optimal area ratio for the nozzle. For this research, however, the outlet pressure will be assumed to be a constant atmospheric pressure at 101325 Pascal. This does not only make the research less complex but also helps in the

comparison of the experimental results as the experiments were conducted at near sea level conditions [11]. Most nozzles used are the converging-diverging de Laval type [6].

The flow of the gas during the converging section is usually small and thus does not account for significant energy loss. However, the contour of the diverging section is crucial as the gas accelerates upon passing through the throat of the nozzle. The selection of an optimal design for the nozzle is vital and determined considering the following goals:

1. Uniform parallel axial gas flow at the nozzle exit for maximum momentum vector.
2. Minimum separation and turbulence losses within the nozzle.
3. Shortest possible nozzle length for minimum space envelope, weight, wall friction losses, and cooling requirements.
4. Ease of manufacturing [6].

Types of Nozzles

1. Conical Nozzles

Conical Nozzles are the most basic type of nozzles. They were widely used in old rocket engines and are easy to manufacture. Existing designs of conical nozzles are easy to modify to higher or lower expansion ratios thus making them easily modifiable. The configuration of a conventional conical nozzle is shown in Figure 3. The nozzle throat section has the contour of a circular arc with a radius R ranging from 0.5 to 1.5 times the throat radius Re. The half angle of the nozzle convergent cone section can range from 20° to 45° [6]. In the divergent section, a 15° half-angle is commonly selected for research studies.

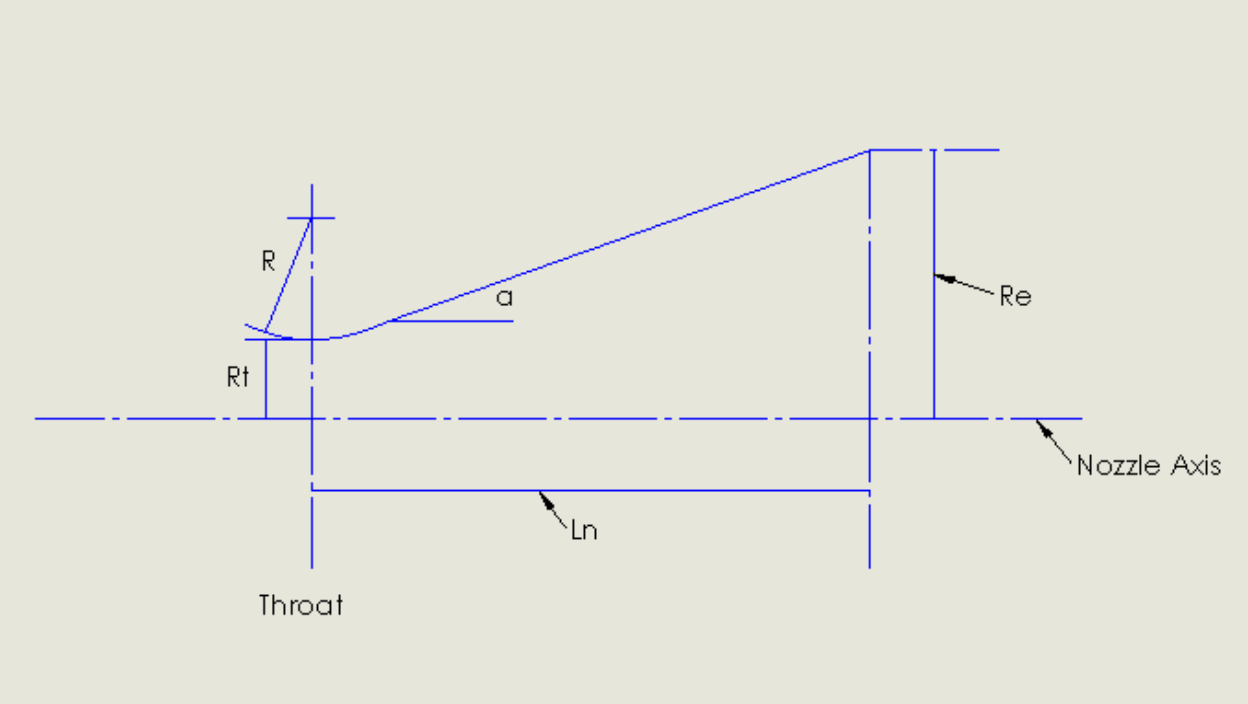

Figure 4. A Conical Nozzle

The length of a conical nozzle can vary according to the equation

$$L_n = \frac{R_t\left(\sqrt{\varepsilon} - 1\right) + R(\sec\alpha) - 1}{\tan\alpha} \quad \ldots(1)$$

Where,

L_n= length of the nozzle

α = half angle of the nozzle

ε = nozzle expansion (area) ratio

R_t= the radius of the throat of the nozzle

R= radius of the curvature of the throat (as shown in Figure 4)

In a conical nozzle, certain performance losses occur. Due to the flow leaving the nozzle at an angle, a correction factor λ is applied for the calculation of the exit gas momentum.

$$\lambda = \frac{1}{2}(1 + \cos\alpha) \qquad \dots (2)$$

This factor would be 1 for an idea nozzle, but for a nozzle half angle of 15°, which is very commonly used, the factor is 0.983 giving 98.3% of the theoretical exit gas momentum [6].

2. Bell Nozzles

Bell Nozzles are used for faster expansions and shorter lengths. A bell nozzle is depicted in Figure 5. Bell Nozzle wall contours are designed in such a way that in spite of the fast expansion, no oblique shocks are formed in the nozzle. On Figure 5, the initial expansion occurs along contour RN after which the flow is redirected to the axial direction by the contour NE. The location of this point E is determined by the expansion ratio and the nozzle length. Usually, the 15° conical nozzle is used as a standard for bell nozzles. For example, a 70% bell nozzle would have 0.7 times the area of a 15° conical nozzle. The comparison is shown in Figure 6. The biggest bell nozzle that can be used efficiently is an 80% bell nozzle. Lengths beyond 80% do not contribute to performance but rather add weight to the system [6].

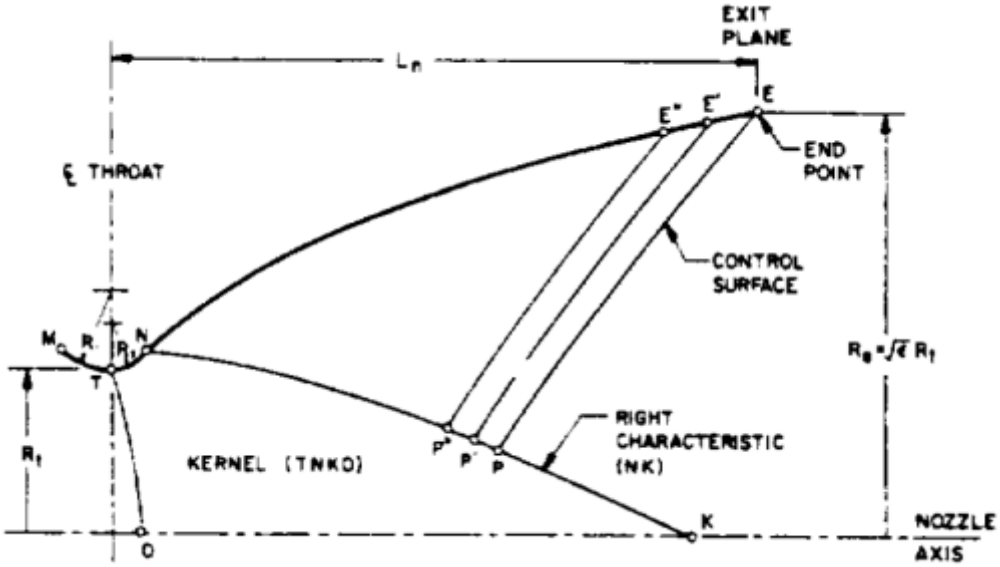

Figure 5. Bell Nozzle Contour [6]

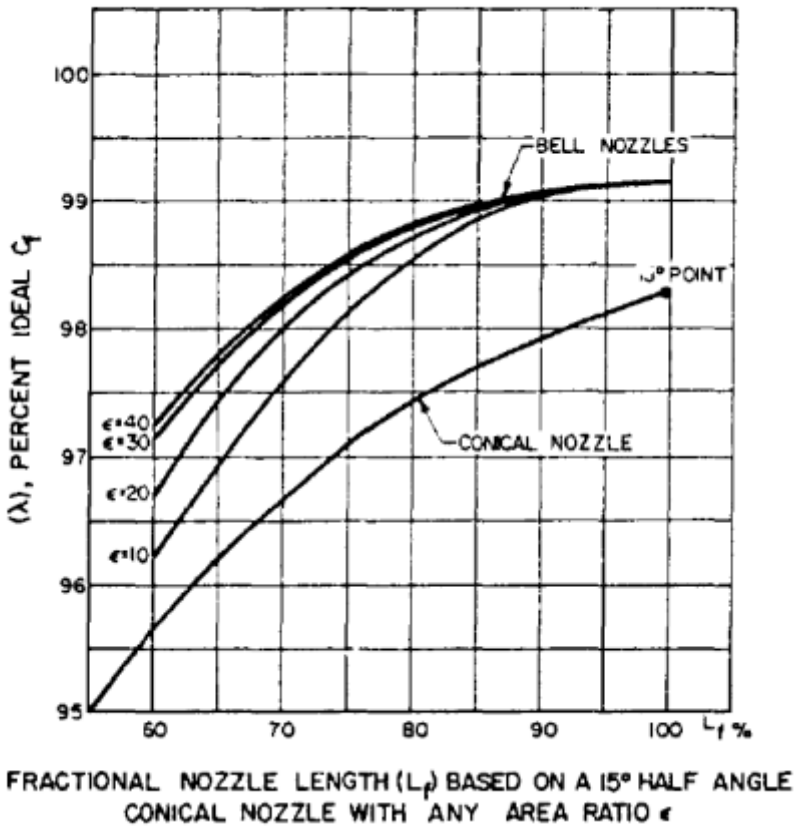

Figure 6. Comparison between Conical and Bell Nozzles [6]

3. Parabolic Approximation of Bell Nozzles

One of the best ways to use a bell nozzle is to approximate it as a parabola as suggested by G.V.R Rao. The design of a parabolic nozzle is shown in Figure 7. The nozzle contour upstream the throat is a circular arc with a radius of 1.5 times the throat radius. The divergent section nozzle contour is made of 0.382 times the throat radius from the throat to the point N as shown in Figure 7. The rest of the nozzle is a parabola up to the exit point E [6].

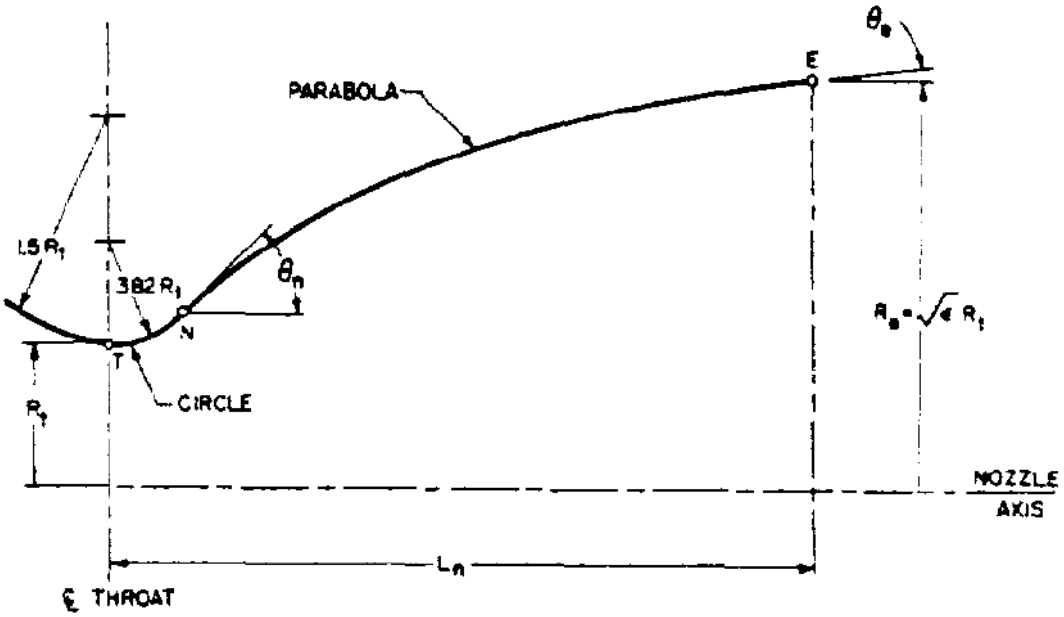

Figure 7. Parabolic Approximation of a Bell Nozzle [6]

For the purpose of this research, a conical and a trumpet bell nozzle will be considered, and their performances will be compared. Attempts will be made to verify Mager [12] and Nortons' [11] analytical and experimental solutions as well.

Conclusion

The introduction of swirl into the flow ahead of the nozzle throat is currently considered in connection with some devices which may prove valuable in rocket engine applications. For example, in certain types of nuclear rockets, the swirl of the spinning propellant has been proposed to retain the heavy uranium atoms inside the rocket chamber [12]. Also, the swirling action is thought to affect the stability and efficiency of combustion and cause a redistribution of the total temperature, which may, in certain cases, lead to the reduction of heat transfer problems. Furthermore, swirling flow is also used in some plasma rockets where this type of flow not only protects the walls of the chamber but also is necessary for arc stabilization. One other device for which the outlet flow is a swirling flow is the bidirectional vortex rocket engine [12]. Since in all these devices the nozzle must necessarily operate with swirling flow, the understanding of such a flow is desirable if their design is to be carried out on any rational basis.

In a fluid flow field flowing with little or no flow turning, the flow is irreversible, and the entropy is constant. But in flows exceeding the speed of sound where there is an abrupt decrease in the area, for example, a nozzle, shock waves may be generated. These shock waves cause a sizable change in the properties of the gas within a very small area. Across a shock wave, the static pressure, temperature, and gas density increases almost instantaneously. In this case, the flow is irreversible, and the entropy of the system increases. These shocks can be harmful to the physical nozzle if unaccounted for during the design and testing of the nozzle [13].

The primary goal of this thesis is to determine the effect of swirl on converging-diverging nozzle performance. To assess this effect, the following areas of interest are proposed:

- Assessment of pressure for two different nozzle geometries.
- Assessment of Mach number to assess the location and intensity of shock structures in the nozzles.

- Comparison of the results with experimental and theoretical results.
- Verify the nozzle design put forth by Talamantes [8] as per Appendix 1.

The first of these proposed assessments will be used to evaluate the effect of swirl velocity on the formation of shock structures within the nozzle. Of particular interest: Does the introduction of a swirl velocity change the strength or location of any shock features in the nozzle? Accurate prediction of these phenomena in standard nozzles is an ongoing area of research. This work will look to extend these studies through the inclusion of a swirl velocity component. The second assessment is focused on assessing steady state nozzle performance. Early theoretical studies have shown that introducing swirl leads to a decrease in the mass flow rate [11,12,14]. Recently, there have been a number of investigations on the effect of swirl on the combustion process in liquid or hybrid motors [15, 16]; however, computational models of swirling nozzle flows do not have the same level of investigation in the literature. This research will help to address that deficiency.

Chapter 2

Methods

Research Purpose

The main purpose of this research is to find the location and intensity of shock structures in a nozzle that has purely axial flow and compare it to that of a nozzle with axial and swirling flow. The nozzle data is taken form the research conducted by Talamantes and Maicke's bidirectional vortex rocket engine [8] as shown in appendix 1 and thus adds as a supplemental tool to their research. The research also aims to verify the reduction in mass flow rate observed by of Norton [11] and Mager's [12] experimental and numerical results respectively using CFD simulations. Two different nozzles geometries are simulated holding the area ratio and the pressure ratio constant.

Research Design

Geometry

The geometries of the nozzles to be used in Star CCM+ were created in the 'geometry' menu of the software itself. Axisymmetric models of the nozzle were created so that the meshes would be created on a 2-dimensional model rather than a 3-dimensional resulting in fewer nodes and smaller processing times as compared to the full 3-dimensional models.

After selecting geometry in the options window on the left, the '3D CAD' option was selected. In the 'features' option the X-Y(Z=0) plane was chosen as the sketching plane. The area ratios of the nozzles (the ratio of the area of the inlet to that of the outlet) and the throat diameters are selected such that they agree with the pressure ratios of the nozzles. These values are determined from appendix 1.

A chamber was created around each of the nozzles to help with convergence. The downstream throat boundary was set at 1.1 m, which is more than 20 throat diameters from the nozzle as per the requirement. Since the nozzle diameter is 5.564 cm, the downstream throat boundary should be at least 160 cm away. The body upstream and perpendicular to the body should be about ten throat diameters away, which is approximately 80 cm. The chamber is then made 1m long downstream of the nozzle. After this, the chamber is completed as shown in Figure 3. A vertical distance is set for the throat using 'apply vertical distance' tool and the parameter is exposed so that the throat diameter can easily be changed to perform the same simulation on nozzles with different throat diameters. An extrude for this sketch is created.

Next, the surfaces of the CAD are named for easy identification and further use. The definition of surfaces is shown in the following Figures. The Figures depict only the conical nozzle mesh structure to avoid repetitiveness.

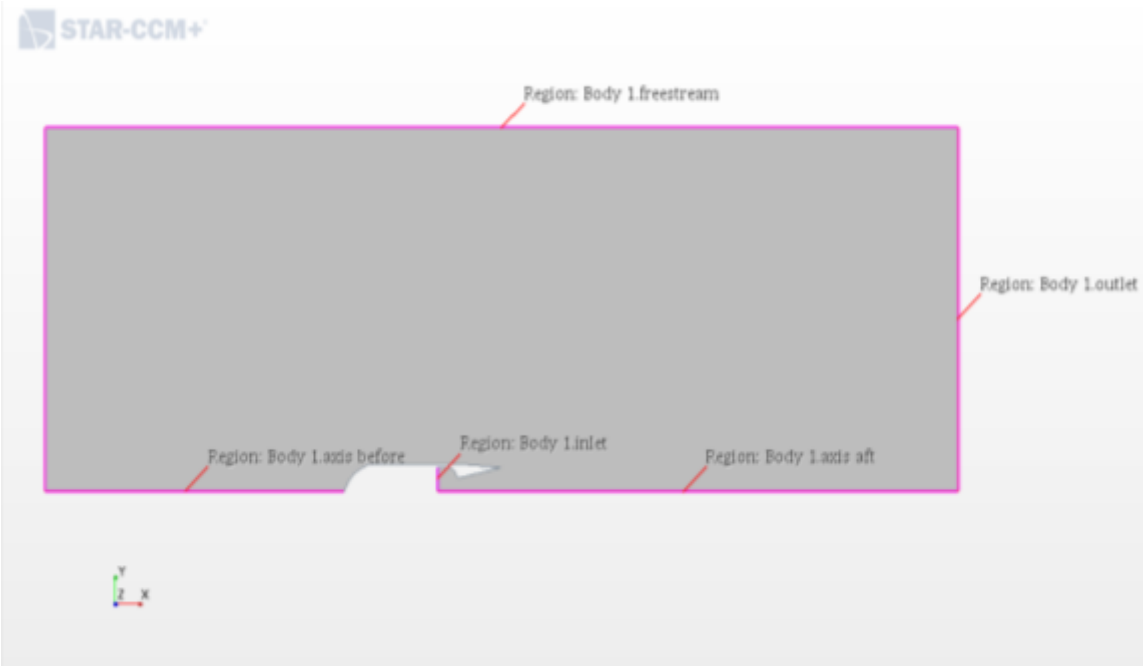

Figure 8. The Computational Domain with the External Boundaries Highlighted

The two surfaces highlighted in pink on the x-axis in Figure 8 are named as axes. The vertical surfaces highlighted in pink at the nozzle inlet and to the right of the fluid domain in Figure 8 are labelled as the nozzle inlet and outlet respectively. The horizontal surface at the top and to the left of the fluid domain in Figure 8 are labelled as 'freestream' as fluid can flow freely through these boundaries.

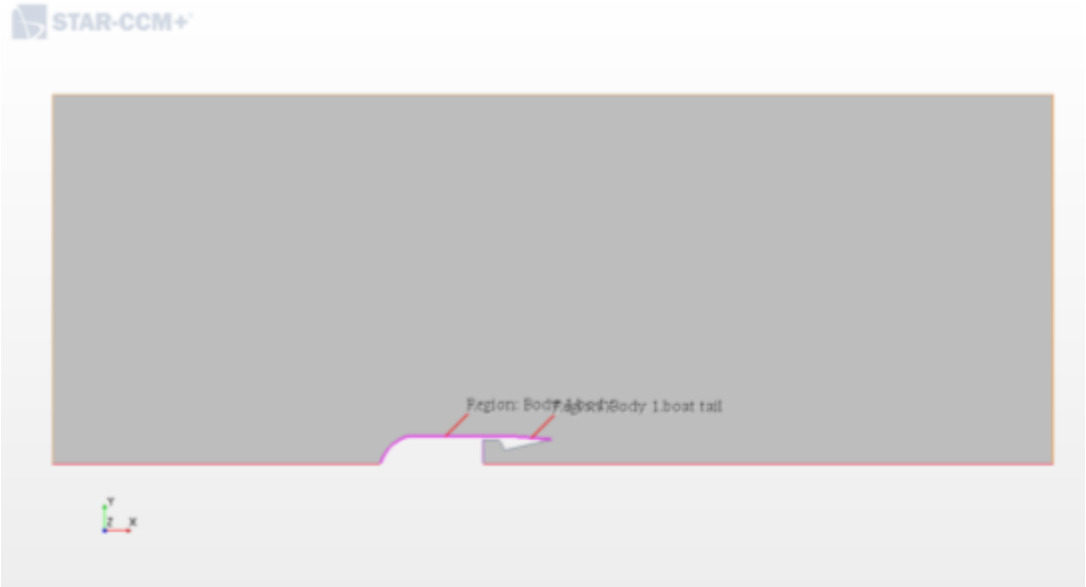

Figure 9. The Computational Domain with Highlighted Boat Tail and Body of the Nozzle

The part highlighted in pink is defined as the body. The inclined surface at the end of the body is named as boat tail as show Figure 9. These surfaces represent the external walls of a rocket.

Figure 10. Computational Domain with Highlighted Nozzle Surfaces 1, 2 and 3

These surfaces are named as nozzle surface 1 2 and 3 respectively as shown in Figure 10. This is done so that different mesh sizes can be set for the three different nozzle surfaces. This body is then transferred to the ‘parts’ option for meshing.

Meshing

Next, in the operations tab, under ‘new’, the ‘create badge for 2D meshing operation’ is selected. This batch is created to identify the geometry in the Z=0 plane. An operation is then created for ‘2D mesh’ using ‘Automated 2D mesh operation’ option. The polygonal meshing option is selected with prism layer mesher. The base size of the mesh cells is set to be 5cm and the minimum size to 100% of the base size. This is done to obtain more accurate results. Under custom controls, in a new control is set for the body and the tail. This is done using the ‘surface control’ option in the ‘custom control’ menu. ‘Surface 1’ is renamed to ‘body and tail’ and the body and tail surfaces are selected. This is done so that we can create a finer mesh for these surfaces as these are the critical surfaces where the major fluid flow activity will take place. In the controls, the target and minimum cell size is set to 10% of the value set as the base size (5 cm) which would thus be 0.5 cm. The number of prism values is also changed to 15 layers and the thickness is set to 15% of the base thickness. Another custom control is set for the ‘nozzle surface 1’, this is simply done by copy-pasting the previous custom control and renaming it ‘nozzle surface 1’. The part under part surfaces is changed to ‘nozzle 1’ from ‘body and tail’. Here only the number of prism layers and the thickness is changed to 20 layers and 7% of the base size respectively. This control is repeated one more time to apply to the nozzle surfaces 2 and 3. Since this is a critical area, the mesh is made very fine such that each cell would be only 1% of the base size or 0.05cm. The

number of prism layers is changed to 25 layers with a relative size of 3%. We then use 2 volumetric refinements, one for the immediate nozzle area and the other for the area after the outlet of the nozzle. Thus 2 volumetric regions are created using cylinders under the ‘parts’ option. A cylinder of radius 12.2 cm is created in the z=0 plane starting at x=-7 and ending at x=50. Another cylinder is created in the Z=0 plane starting at x=7 and ending at x=200 with radius =7.2 cm. These volumes are used for volumetric refinements with sizes of 5% and 10% of the base size for cylinder 1 and cylinder 2 respectively. The critical region is this finely meshed to obtain accurate results. The mesh is now set up and created by clicking on the ‘mesh’ icon. Figure 11 shows the mesh.

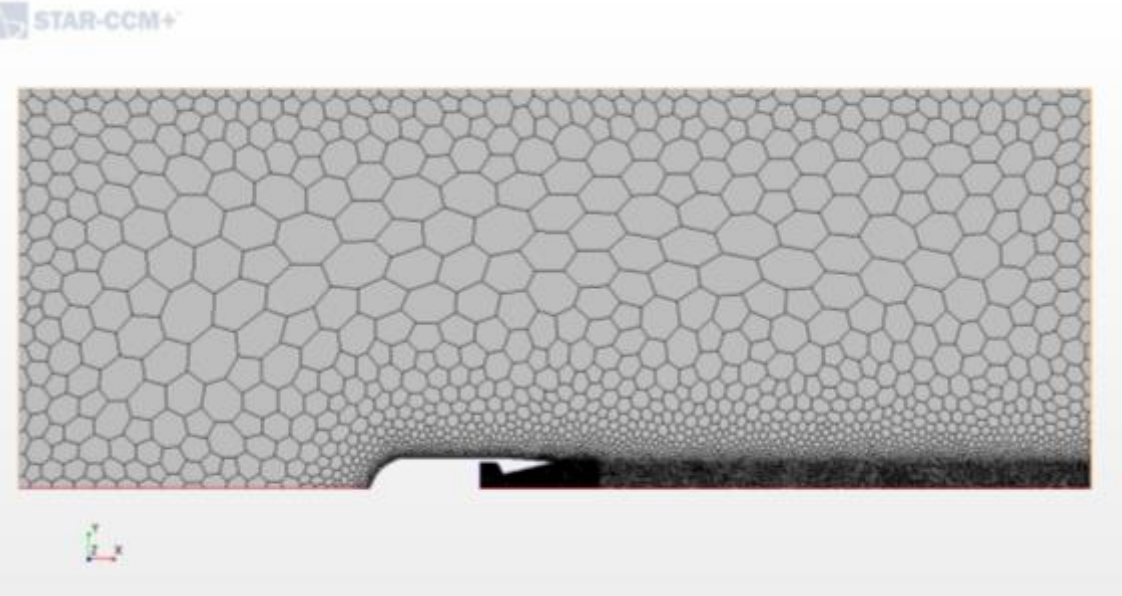

Figure 11. Polyhedral Mesh Generated in Star CCM+ for a Conical Nozzle

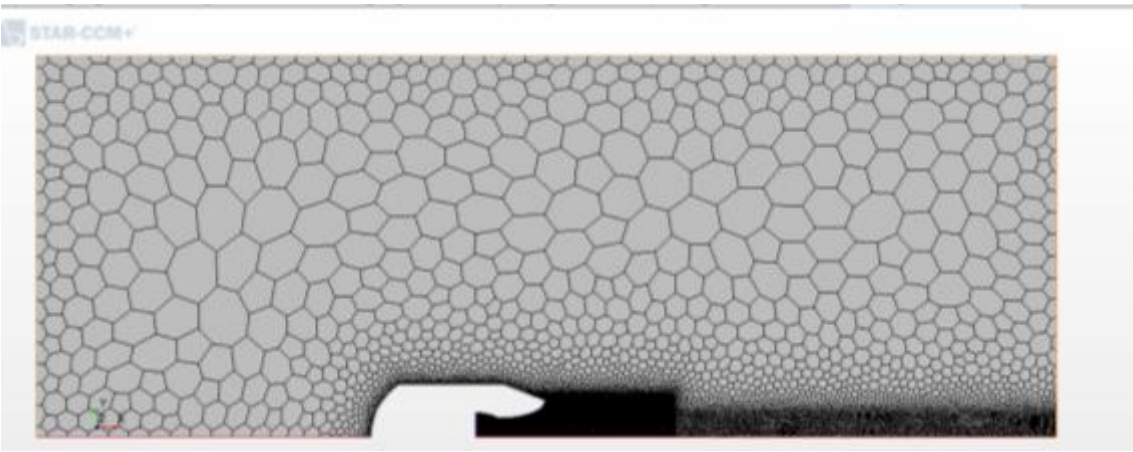

Figure 12. Polyhedral Mesh Generated in Star CCM+ for a Parabolic Nozzle

Physics and Setup

Setup for non-swirling flow

Under parts in the body option, the 'assign parts to region' option is selected this is done to create a boundary for each part surface so that different physics can be applied to different parts of our body. Under the 'Continua' node, the physics for the simulation is set up. Axisymmetric space is selected, the time to be at steady state, the material to be gas, the flow to be coupled flow, the equation of state as Ideal Gas, the Viscous regime to be 'Turbulent' and the turbulence model to be 'K- Omega Turbulence'. The coupled inviscid flux is set to AUSM+FVS under the 'coupled flow option'. In the 'reference values' tab, the minimum temperature is set to 50K from 300K. A few changes are then made under the 'initial conditions' tab.

The pressure inside of the nozzle and upstream of the throat is initialized to chamber pressure for added numerical stability. To do this, a field function is created by selecting the field function option for the initial condition 'pressure'. Under tools, a scalar field function is created titled 'Pressure_Initial'. The initial pressure is set to 1998675 Pa inside the part of the nozzle before

the throat as determined from appendix 1. This is done so that the boundary initial condition is not very different from the initial conditions inside the nozzle. Since boundary conditions are treated by the solver as a special case, having a big pressure difference at the boundary could potentially cause problems with the solver. This field function is then set as pressure under the 'initial pressure' node. The initial velocity is adjusted to 427.2 m/s in the X-direction. This value for axial velocity is used such that the total kinetic energy provided to the system is the same in both swirling and non-swirling cases.

In the regions node, the boundary type is changed for each surface from the default setting of wall. The 2 axes are set as axis type boundary, the 'freestream' as free stream, the 'inlet' and stagnation inlet and the 'outlet' as pressure outlet. Nozzle 1 2 and 3 are left unchanged as they are of the default 'wall' type. For the body inlet, the initial pressure is set to the combustion chamber pressure which in this case is 1998675 Pa and the inlet temperature is set to 500K. All the other initial conditions are left unchanged.

Under solvers, the 'expert initialization' is set to grid sequencing, this solves a series of inviscid solutions to better initialize our simulation. The maximum grid level is set to 10, the maximum iterations per level set to 100, convergence tolerance is set to 0.01 per level and the CFL number of 3. The solution driver is set to 'expert driver' without any changes to the default settings, so that during the run, the Courant number is automatically adjusted. The case is let to run for 5000 iterations or until cyclic residuals are obtained.

A 'Mach Number at Inlet' surface average report under the reports tab is created to monitor the Mach number at the stagnation inlet upstream of the nozzle. If the CFL number is too high or the initial conditions are set incorrectly, the Mach Number can go above 1 on this face which could cause potential convergence problems. Thus keeping a track of this report is important. The value

of Mach Number at inlet is plot and would be displayed throughout the run. Scalar and vector scenes can now be created for different results that need to be obtained such as ‘Mach Number’, ‘Pressure’, ‘Velocity’, ‘Mass Flow Rate’ etc. The simulation is then run to get the results.

Setup for swirling flow

For introducing a swirling flow in the nozzle, the only changes that have to be made are in the models section, where axisymmetric swirl is selected as a solver model. This allows a z-coordinate for velocity to be set which causes the flow to swirl. In the ‘initial conditions’ the velocity at the inlet in the z direction is set to be 400 m/s. To keep the net velocity equal to that in the axial flow case (427.2 m/s), the axial velocity in this case is changed to 150m/s. In ‘boundary conditions’ for the inlet the z-direction component is set to 1 so that continued velocity in the z direction is provided at 400m/s after initiating the flow.

Chapter 3

Star CCM+ Simulation for Conical Nozzles

Since Star CCM+ is a software with a lot of commercial uses and is considered to be reliable, a working CFD model of the nozzle was expected with both swirling and non-swirling flow for accurate comparison. The conical nozzle has an easier geometry for the Star CCM+ solver as compared to that of the parabolic nozzle as shown in Chapter 4, thus it can be said the more accurate results were obtained in this section as compared to the previous one. The results have been categorized in the sections as Residuals, Mach Number, Pressure, Density and Average Mass Flow Rate at Outlet.

Residuals

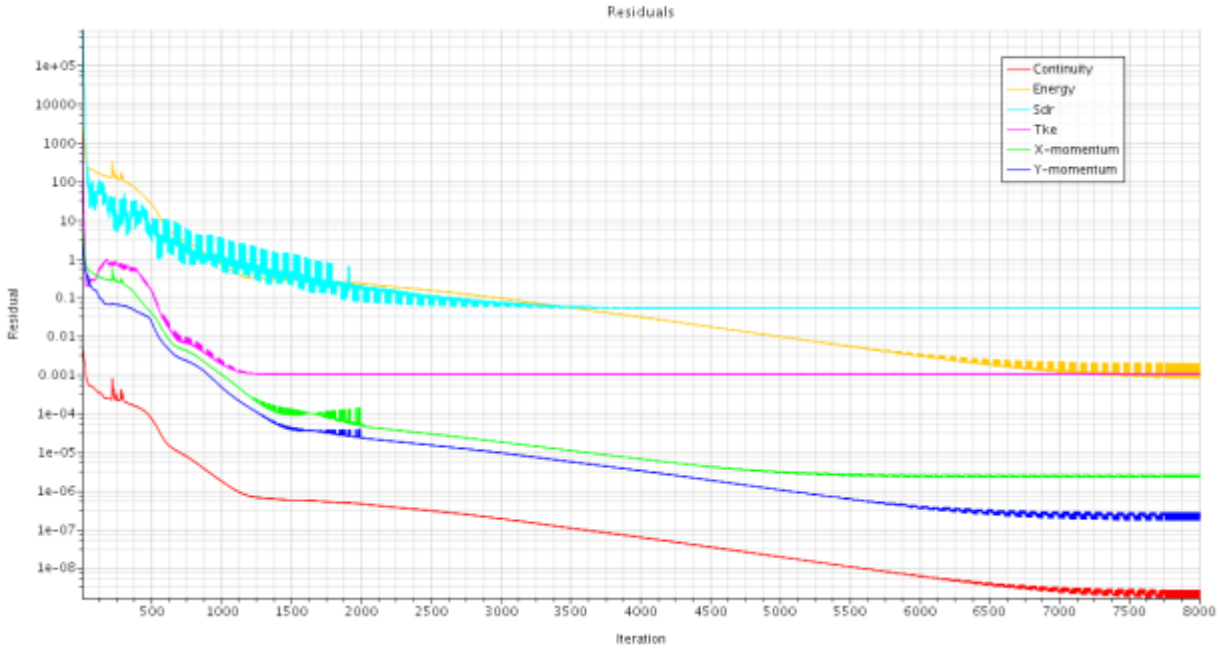

Figure 13. Residuals No-Swirl

The simulation corresponding to the above residuals was run for 8000 iterations against the stipulated 5000 as the results were still converging and were not cyclic as in other simulations at 5000 iterations, thus making the results more accurate. As it can be seen from Figure 13, the convergence in X-momentum, Y-momentum and continuity is well below 0.0001. This shows that as the software was performing the simulations, the difference between the value calculated in the previous iteration and the value calculated during the current simulation is less than 0.0001, thus giving us accurate results. The Energy and Tke (Total Kinetic Energy) of the system converged just below 0.01 whereas the Sdr converges to around 0.1.

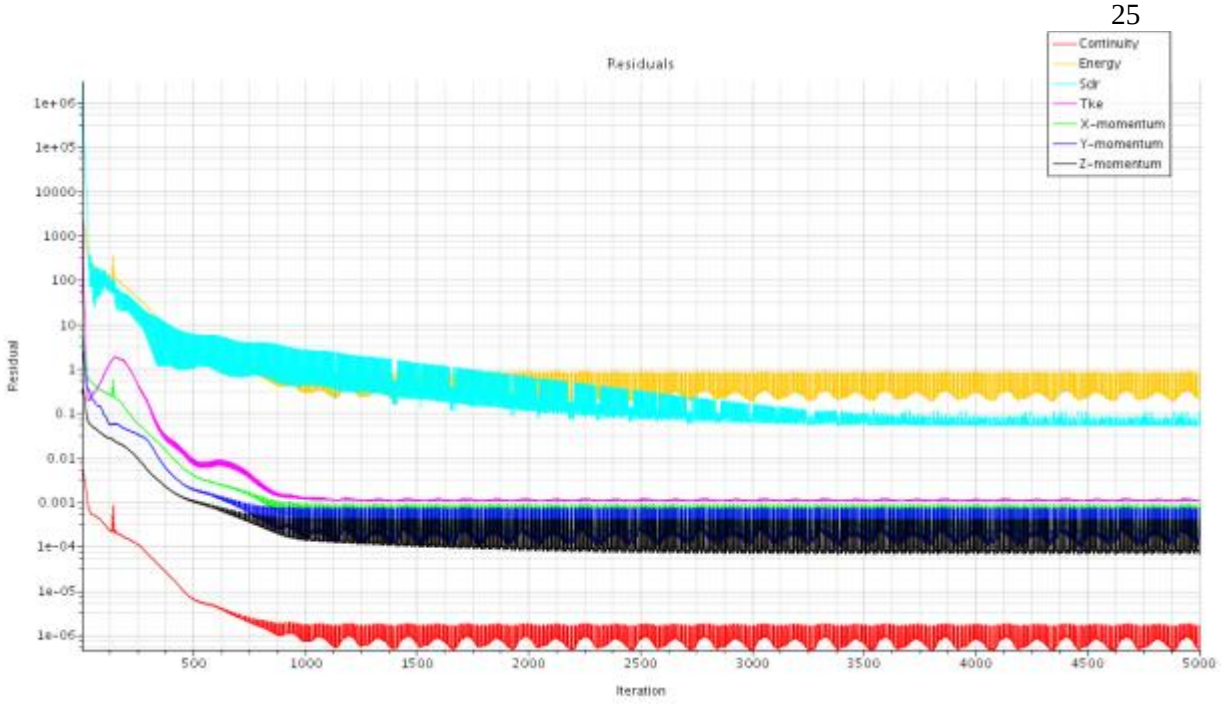

Figure 14. Residuals Swirl

The simulation corresponding to Figure 14 was run for 5000 iterations as per the guidelines set in chapter 2 after which the solver was stopped as the residuals became cyclic and repetitive. As in the previous simulation the Continuity converged to well below 0.0001 but the convergence in the X and Y momentum was not the same as in the case without any swirling fluid. This can be caused due to the uncertainty caused by the swirl that would add an extra component to the flow. Similarly, the energy does not converge as well as in the previous case having a maximum value close to one at 5000 iterations and the Total Kinetic energy (Tke) converges very close to 0.001, but not as well as in the non-swirling flow case. The reason for this can also be associated to the extra component of velocity in the flow through the nozzle.

The residuals of this simulation also show the Z momentum as the simulation has flow in the Z direction too (the swirl component) as opposed to flow in only the X and Y directions in the case of axial flow.

Mach Number

Mach Number Contour

The images below describe the Mach number contours at different points in the nozzle. The Mach number is the ratio of the speed of the fluid particles to the speed of sound at that location. A dual shock pattern can be seen in both Figure 15 and 16 which is further verified by the pressure scatter plot in Figure 21 and 22 showing two bumps in the pressure scatter, one at X=0.35m and the other at X=0.74m.

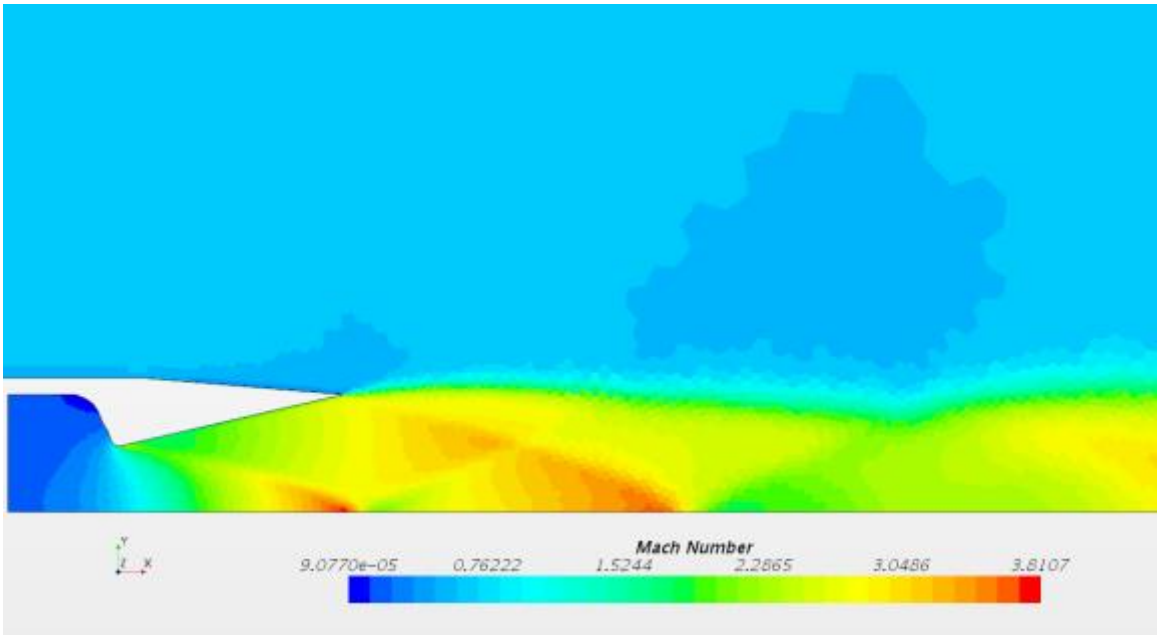

Figure 15. Mach Number Contours of Non-Swirling Fluid

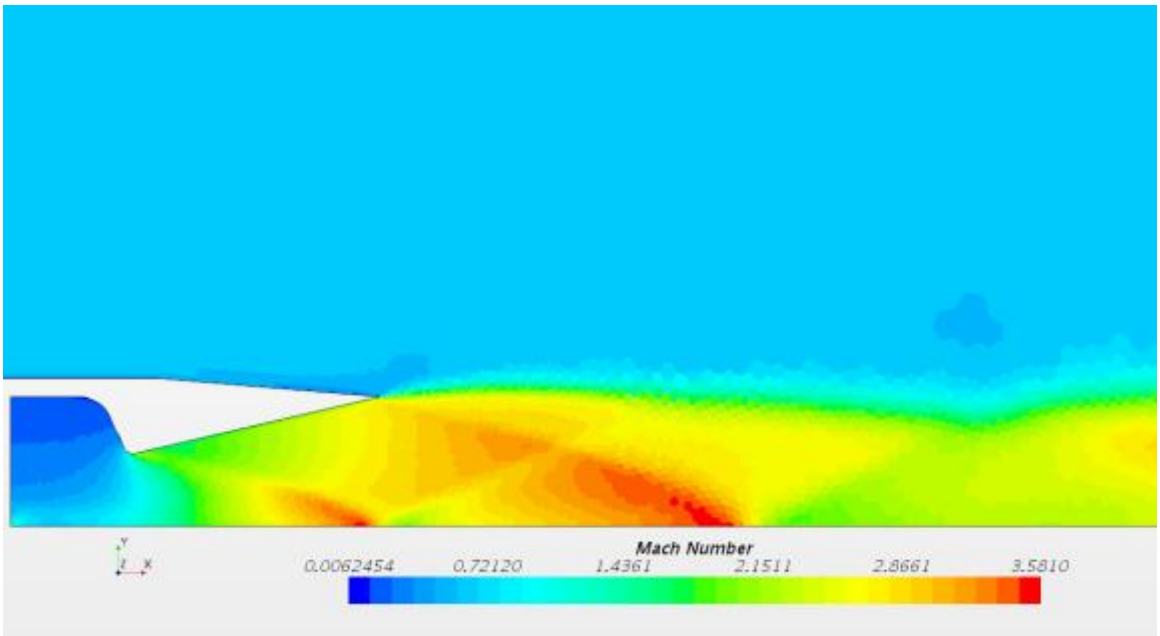

Figure 16. Mach Number Contours of Swirling Fluid

Even though the location of shocks in the two pictures is identical (further verified in Figures 17 and 18), the intensity of shocks is different as it can be seen from the difference in the Mach number contours in Figures 15 and 16. The coloration of the scales in the two Figures represents two different values which can be misleading, however it can clearly be seen that the maximum Mach number in the swirling flow case in much lesser than that in the non-swirling flow case. It can thus be hypothesized that the drop in Mach number for swirling fluid across a shock is smaller as compared to that of a non-swirling fluid.

Mach Number Scatter

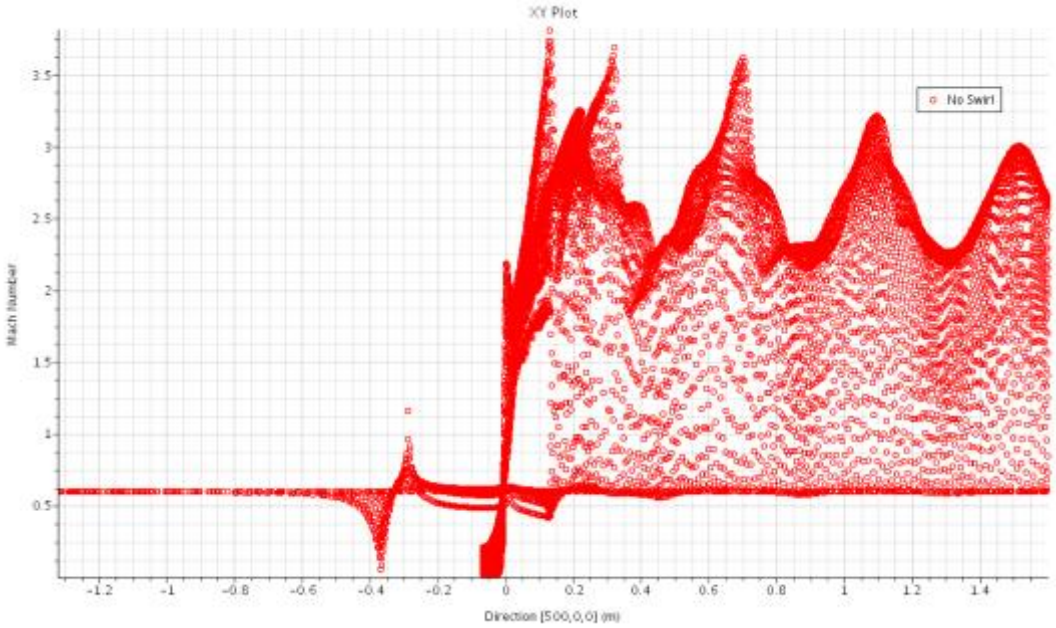

Figure 17. Mach Number Values(scatter) with Respect to the x Axis for Non-Swirling Fluid.

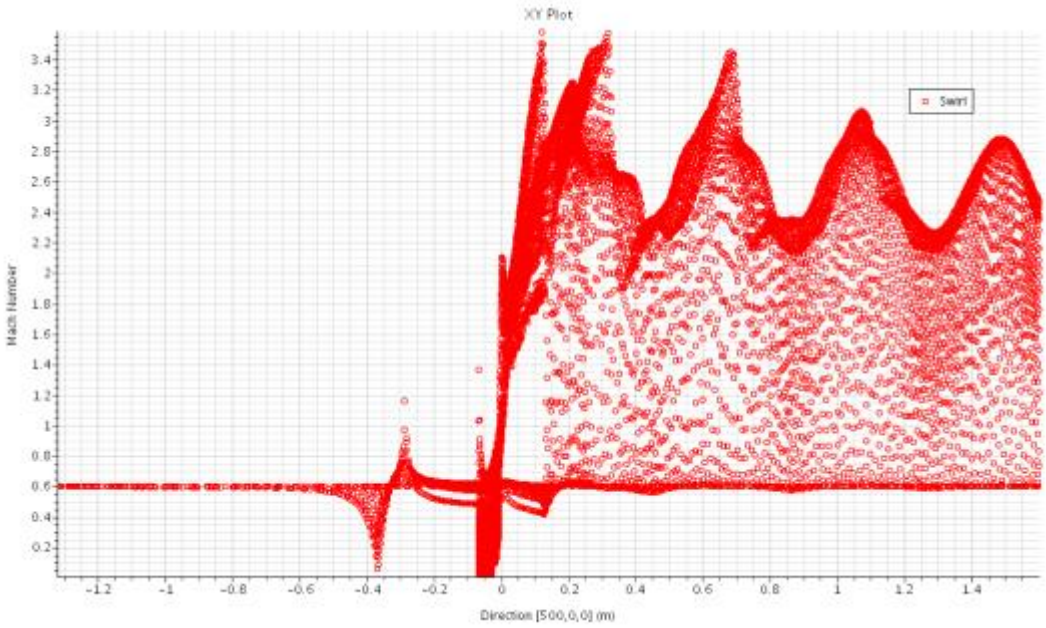

Figure 18. Mach number Values(scatter) with Respect to the x Axis for Swirling Fluid.

A scatter of the two flows is plotted with respect to the x axis. It is found that the location of the shocks in the two figures are identical but the intensities are different. The Mach number scatter plot with swirling flow has scatter points with a higher Mach number than the one without swirling fluid. As per the geometries of the nozzles, the nozzle throat is located at point x=0 with the nozzle exit being close to x=0.16m. Thus, it is evident that the shock is downstream of the nozzle, outside the nozzle body.

Pressure

Pressure Plots

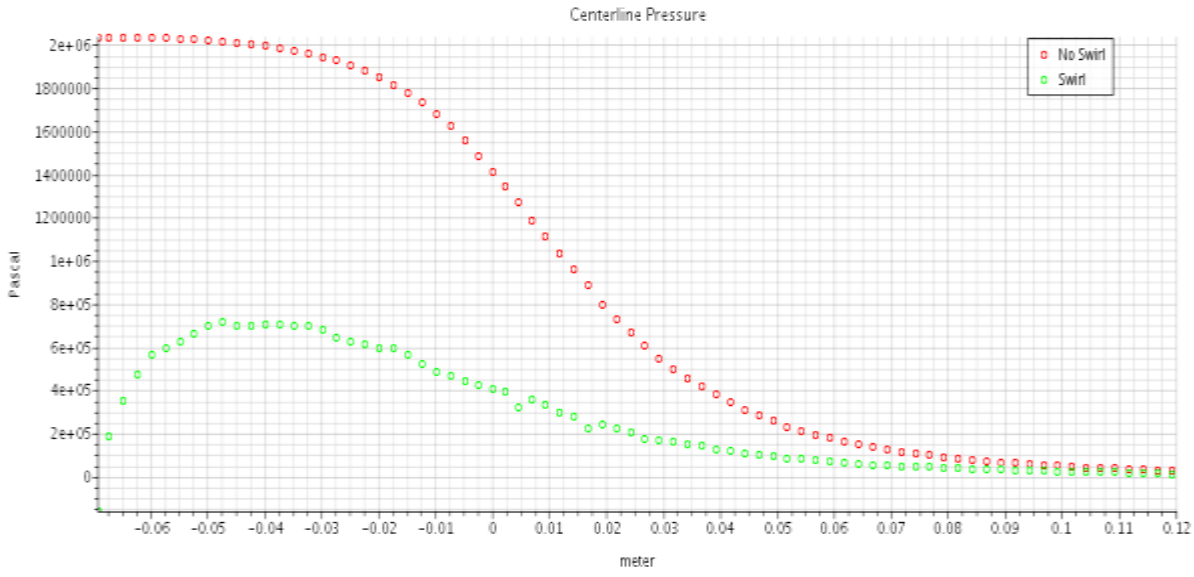

Figure 19. Pressure at the Centerline of the Nozzle

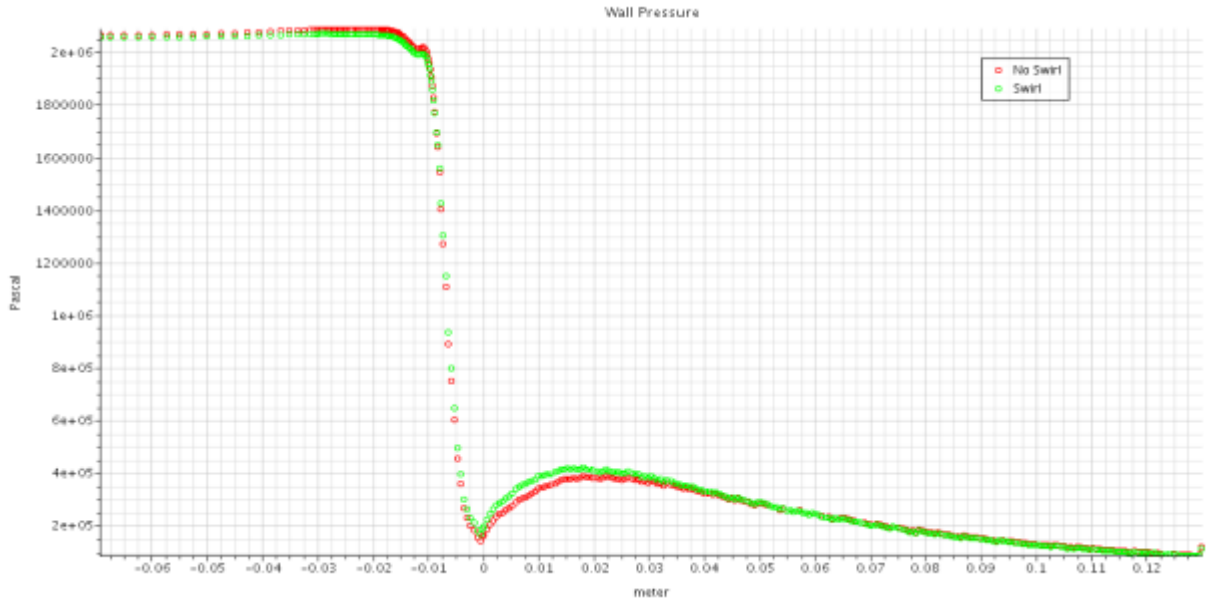

Figure 20. Pressure at the Wall of the Nozzle

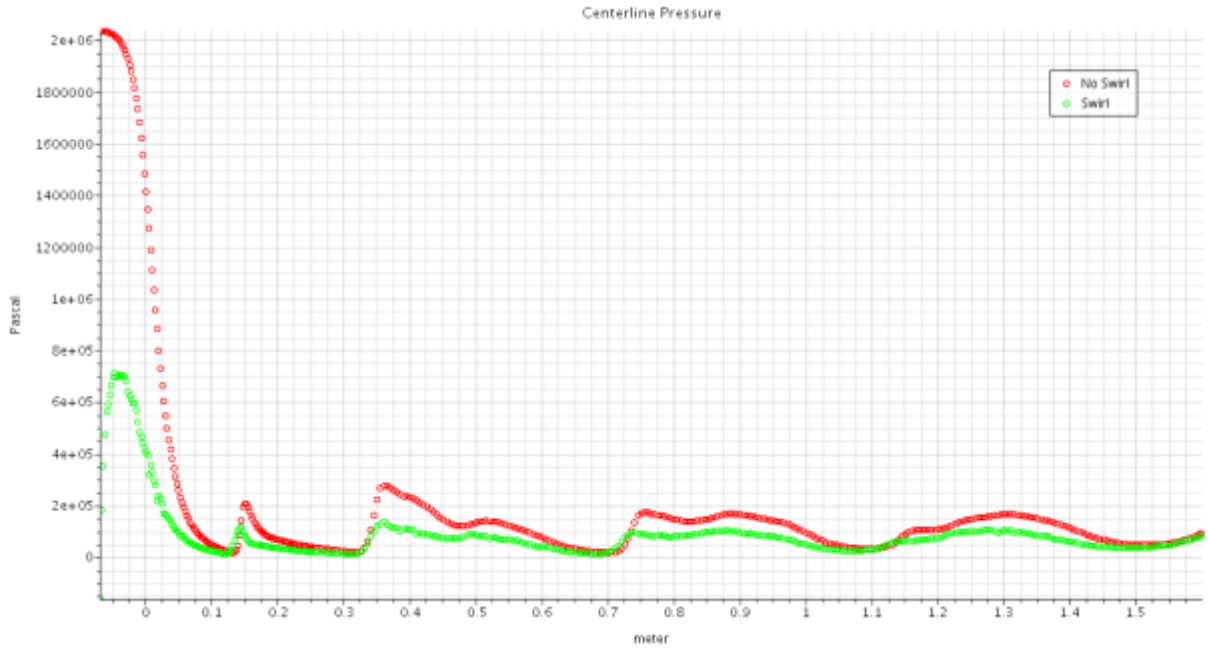

Figure 21. Pressure Along the Symmetry Axis of the Nozzle Body

Figures 19 and 20 show the variation of pressure between the 2 types of flows at the centerline axis and at the wall. The red scatter represents the non-swirling fluid nozzle while the green line represents the swirling fluid flow nozzle.

There is noticeable difference between the pressure at the centerline but little difference at the wall. In fact, the pressure at the walls is higher for the nozzle with swirling flow for certain values of x. This can be attributed to the fact that in a nozzle with a swirling flow, the centrifugal force experienced by the particles would cause the particles to go outwards, towards the wall of the nozzle, thus creating a relatively low pressure region at the centerline of the nozzle. This effect would then diminish going further away from the nozzle as is evident from Figure 20 and 21 due to the effect of the swirl diminishing as we go away from the inlet.

Pressure Scatter

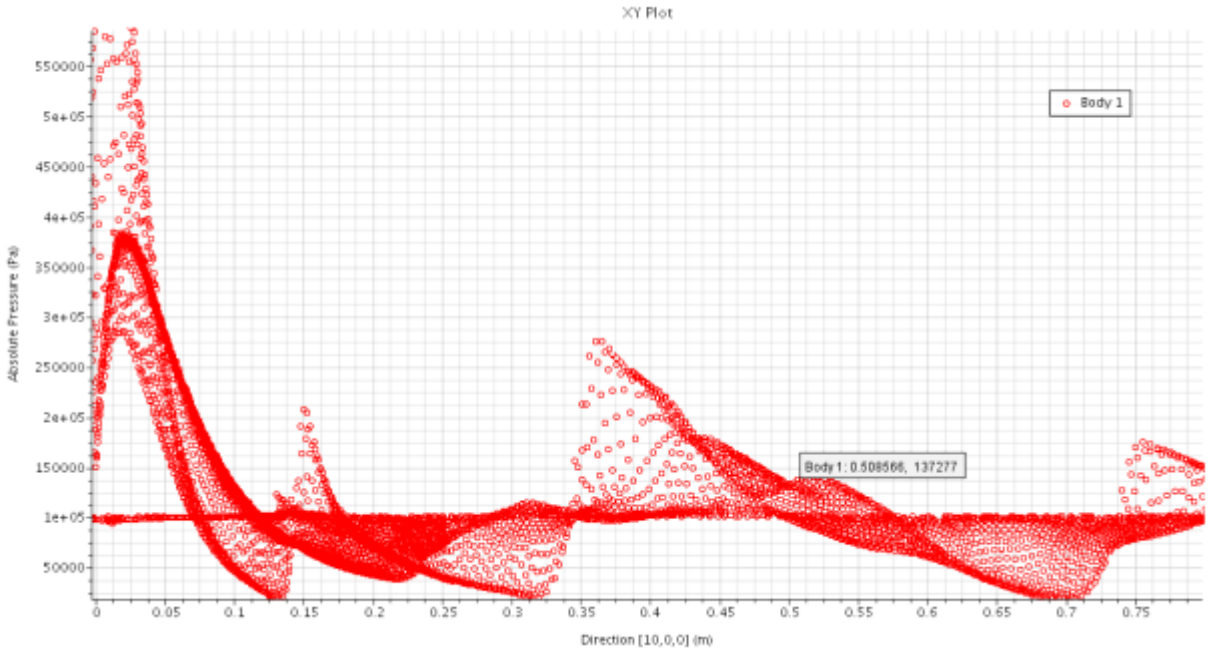

Figure 22. A Scatter Chart for the Various Pressure Values for Non-Swirling Flow

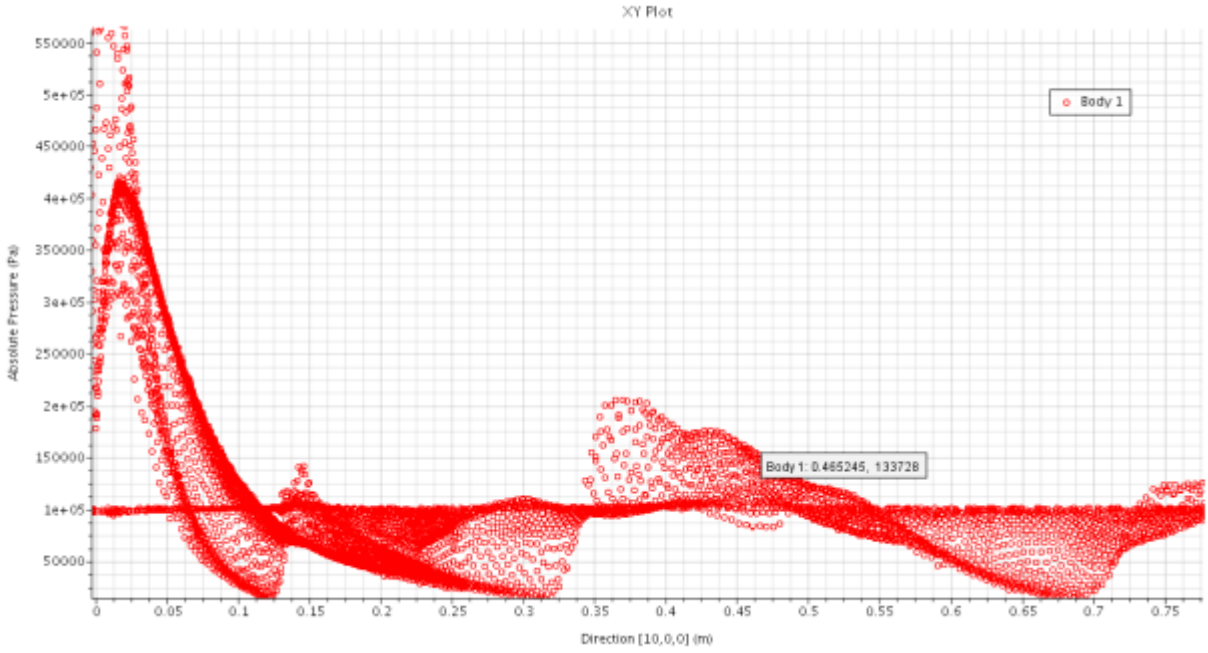

Figure 23. A Scatter Chart for the Various Pressure Values for Swirling Flow

To further verify the results and prove the hypothesis in Mach number section, pressure scatter is plotted with the x-axis in Figures 22 and23. These plots clearly show a higher drop in pressure at the shock locations of x=0.35m and x=0.74m in the case of non-swirling flow as compared to that of swirling flow. This is consistent with the hypothesis set forth in the Mach number section of the results

Density

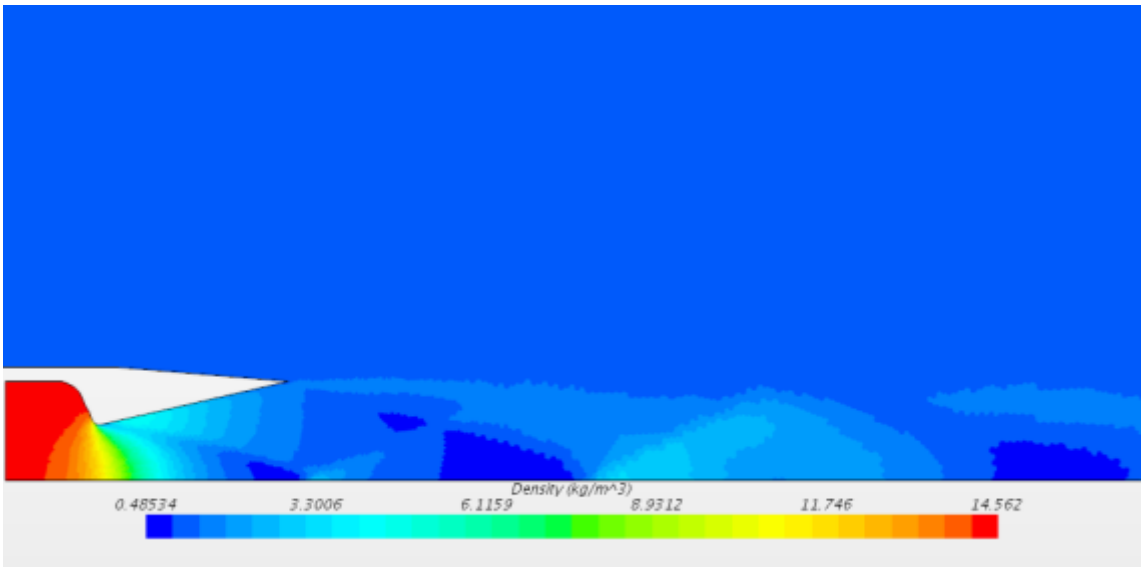

Figure 24. Density Contours of Non-Swirling Fluid

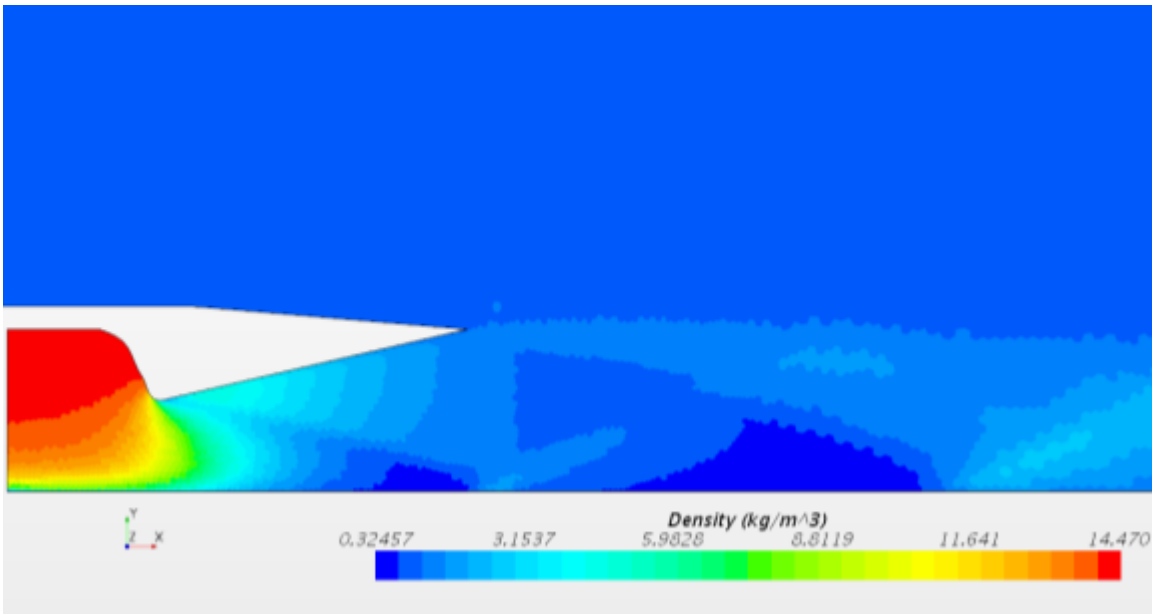

Figure 25. Density Contours of Swirling Fluid

The density plot shows the fluid density at different points in the nozzle considering the fact that the solver was set to compressible flow solver, allowing the density to vary from point to point. As it can be seen from the figures, the density in the case of swirling flow is lower than that

in non-swirling flow. The density in Figure 24 also shows the flow to be concentrated around the centerline axis whereas the density in the case of swirling flow is pushed more towards the wall thus increasing the pressure in the region as per Ideal Gas Law as shown in Figure 25, which further verifies the results in the Pressure section.

Mass Flow Rate at Outlet

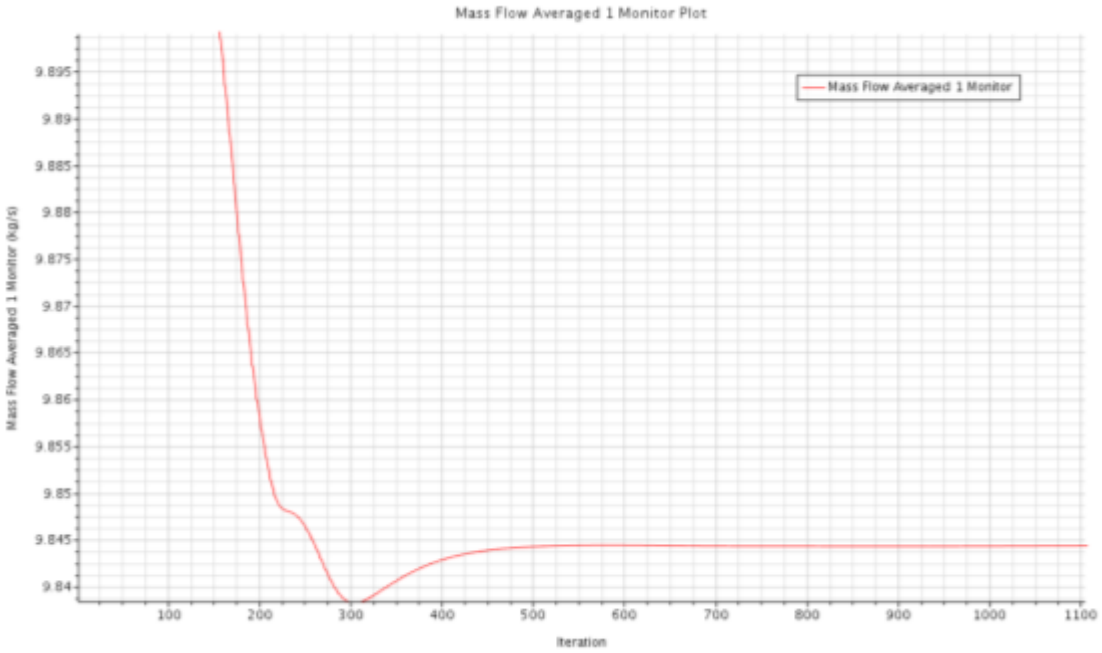

Figure 26. Average Mass Flow Rate at Outlet for Non-Swirling Fluid

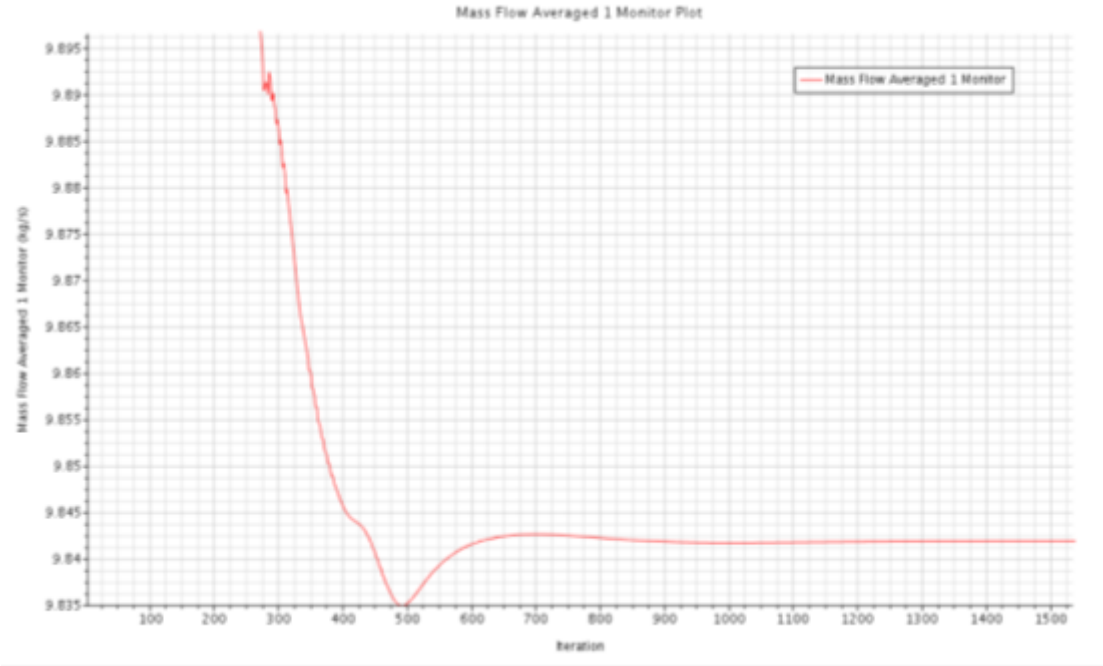

Figure 27. Average Mass Flow Rate at Outlet for Swirling Fluid

Another important aspect of this research was to determine and compare the mass flow rates of the two types of flows when all the other conditions were unchanged. Even though the results in this regard were not very convincing, preliminary data could be obtained. Figures 26 and 27 show the average mass flow rates at the outlet for the two types of flows. Simulations show that the mass flow rate for the fluid without swirl is slightly higher than the one with swirl. The value of the mass flow rate in the non-swirling case was close to 9.845 while in the swirling flow case was close to 9.842. This is in agreement with the results presented by A Mager in his research [11].

Chapter 4

Star CCM+ Simulation for Parabolic Nozzles

The simulations in the parabolic nozzle were run in a similar manner to the ones in the case of the conical nozzle. A trumpet-bell nozzle was used where a deflected cantilever beam forms the nozzle wall. This kind of nozzle is used for academic research as an adjustable exit area nozzle [17]. Some of the results obtained in this section were in agreement with the results in the case of the conical nozzle while the others show significant differences. The results are further discussed in this section.

Residuals

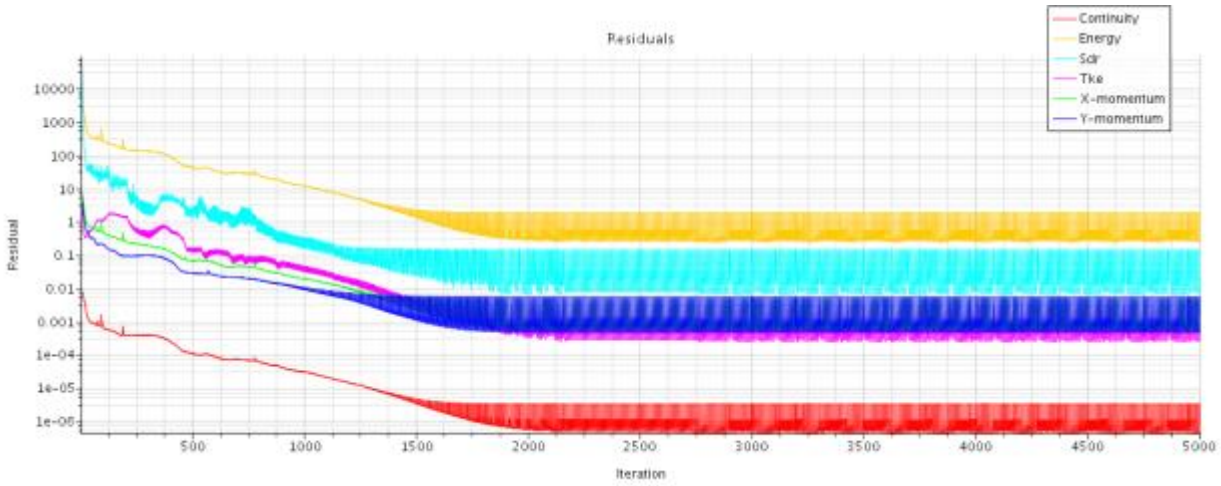

Figure 28. Residuals No-Swirl

As it can be seen from Figure 27, the convergence in X-momentum Y-momentum and Tke (Total Kinetic Energy) is below 0.1 and continuity is well below 0.0001. The Sdr of the system

converged just below 1, whereas significant error can be seen in the results in the case of Energy, which converged to just below 10 but above 1. This can be attributed to some features of the nozzle geometry discussed further in this section.

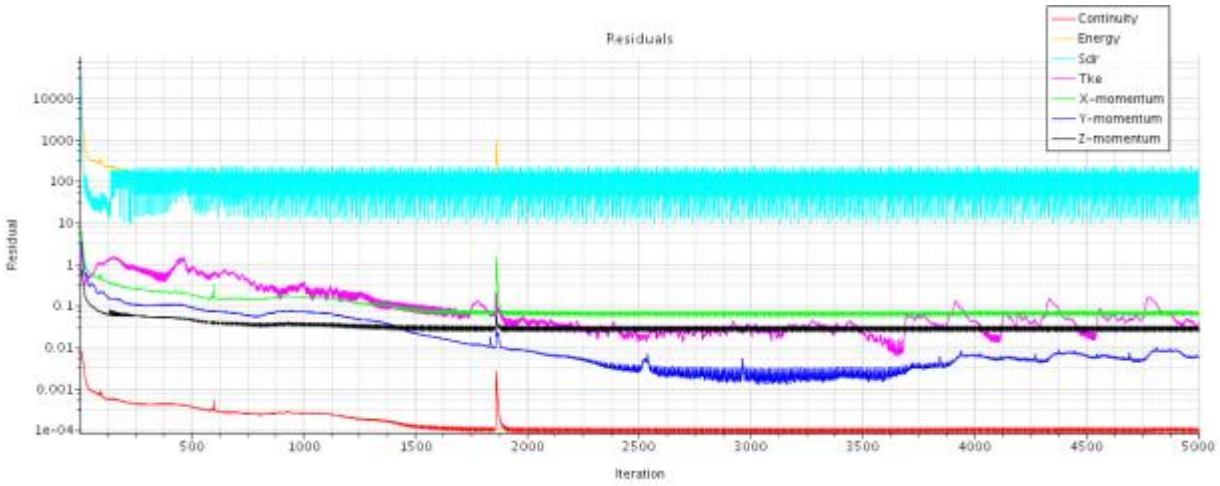

Figure 29. Residuals Swirl

As in the previous simulation the Continuity converged to well below 0.0001 but the convergence in the X and Y momentum was not the same as in this non swirling flow case. Even though the Y momentum converged close to 0.01, the X and Z momentum converged close to 0.1. The convergence in energy and Sdr is approximately a 100 which appears to be a considerable amount of error in the results. However, relative residual settings were used for the simulations, meaning that they are the ratio of the current residual error to the error near the beginning of the simulation. Thus the values in the residuals shown can be relatively smaller depending on the values of the residuals in the beginning of the simulation.

Mach Number

Mach Number Contour

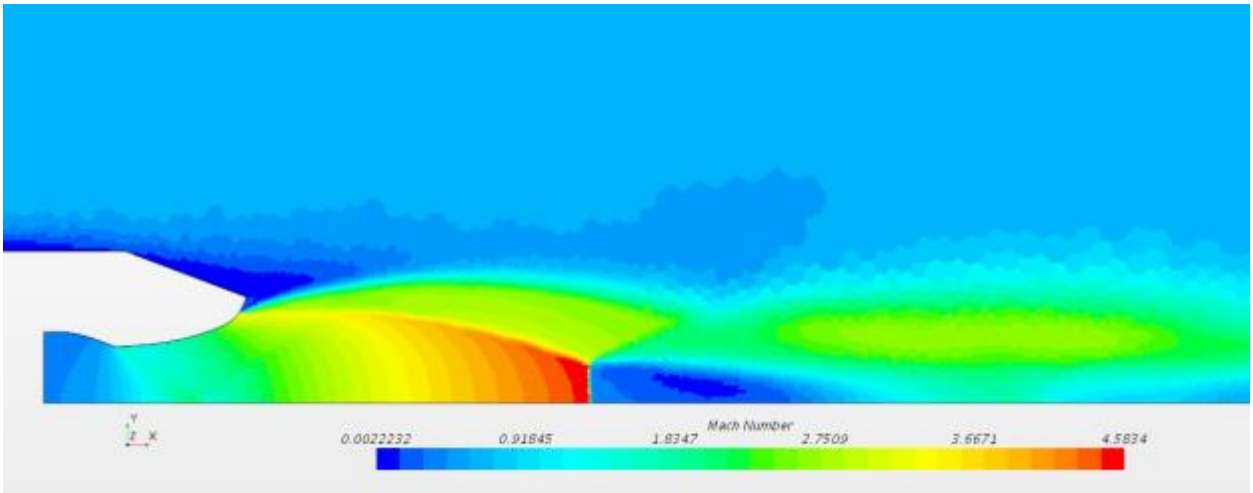

Figure 30. Mach Number Contours of Non-Swirling Fluid

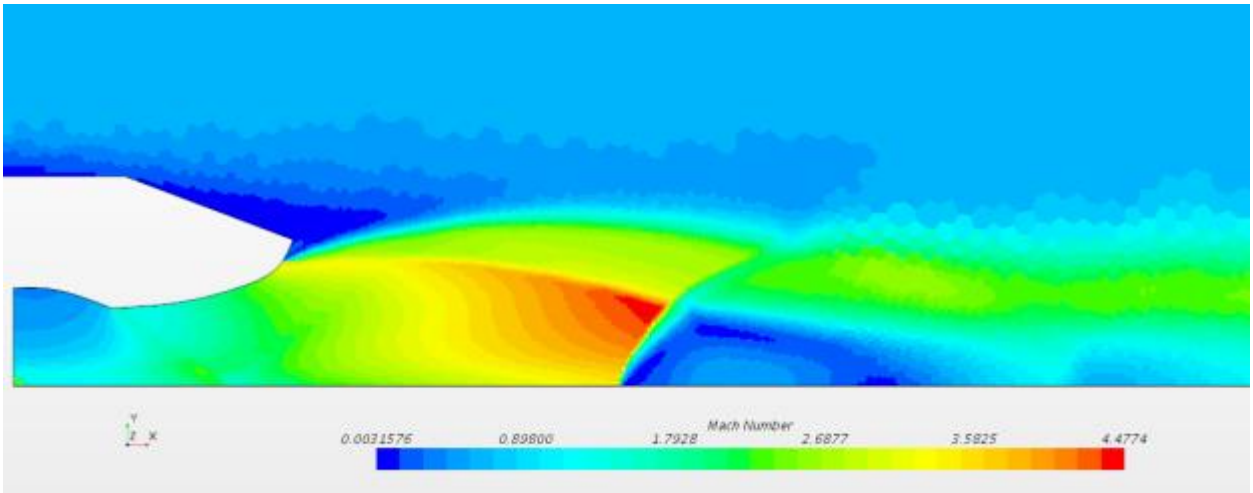

Figure 31. Mach Number Contours of Swirling Fluid

The Mach number contours agree with the conical nozzle and the experimental and theoretical results. The Mach number in the swirling flow case is much smaller than that in the

non-swirling flow case. Also, the shock appears to be much more gradual than in the case of the swirling flow case. It can also be seen that the shock location is different for the two cases. There is also a slight difference in Mach number at the exit as the parabola has a continuously increasing contour.

Mach Number Scatter

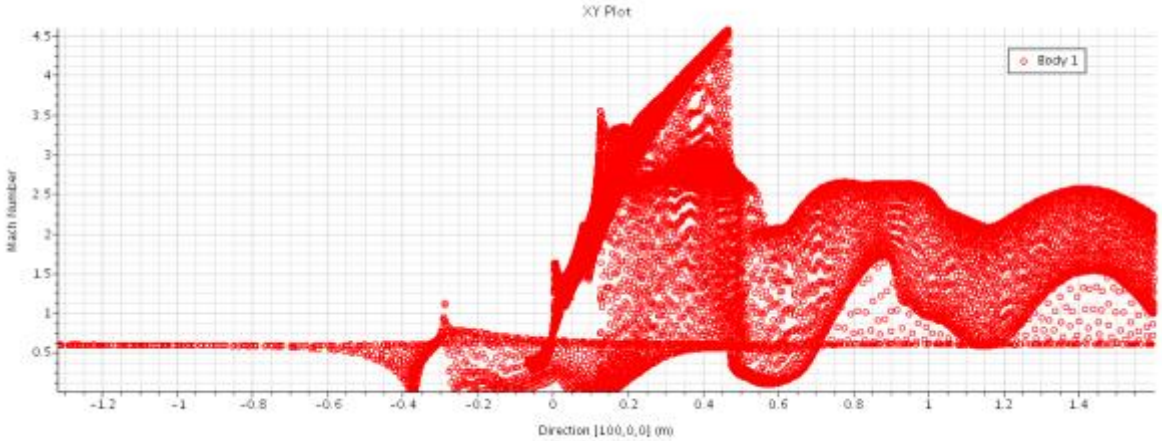

Figure 32. Mach Number Values(scatter) with Respect to the x Axis for Non-Swirling Fluid.

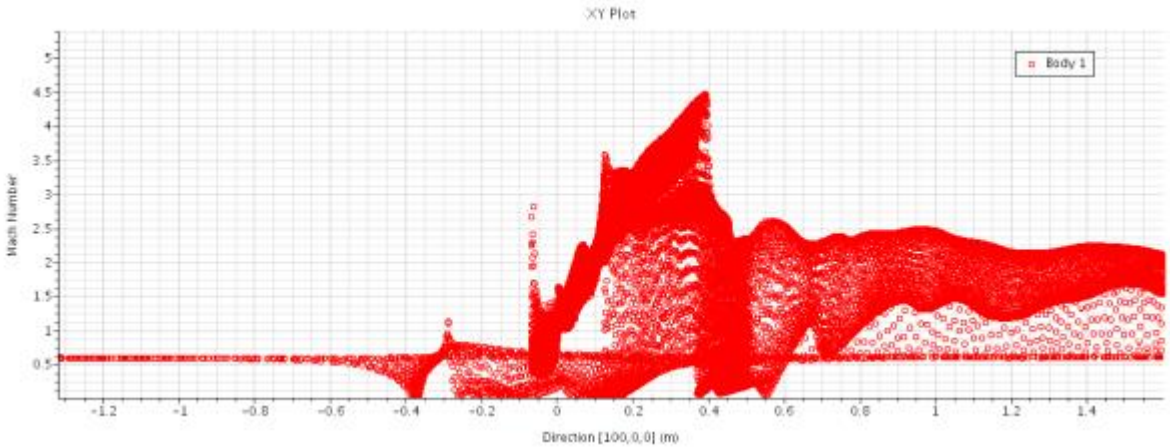

Figure 33. Mach Number Values(scatter) with Respect to the x Axis for Swirling Fluid.

The scatter plot of the Mach numbers shows a higher Mach number in case of the non-swirling flow thus in agreement with the results in the conical nozzle section. Difference can however be seen in the location of the shock, where the shock occurs closer to nozzle on the case of swirling flow as compared to the case of non-swirling flow. It is possible that the trumpet-bell profile is more strongly affected by swirl. There is however a possibility that the change in the location of shock can be a result of the error as shown in the residuals. More work is needed to validate the result.

Pressure

Pressure Plots

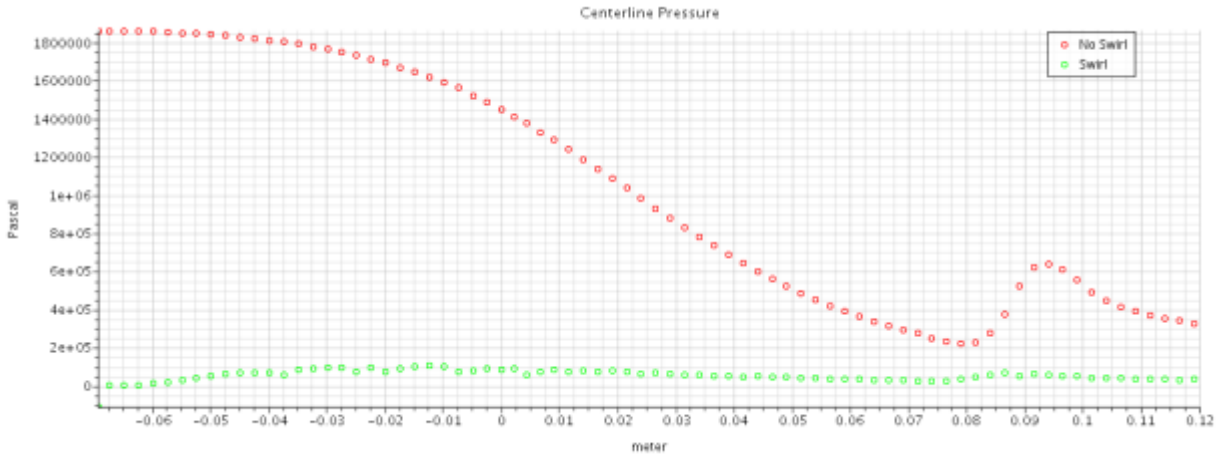

Figure 34. Pressure at the Centerline on the Nozzle

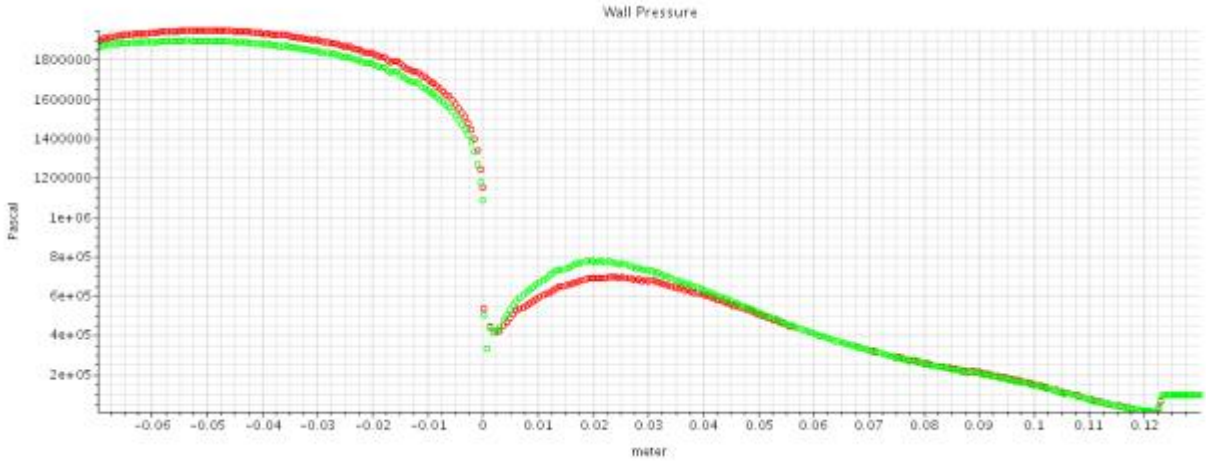

Figure 35. Pressure at the Wall of the Nozzle

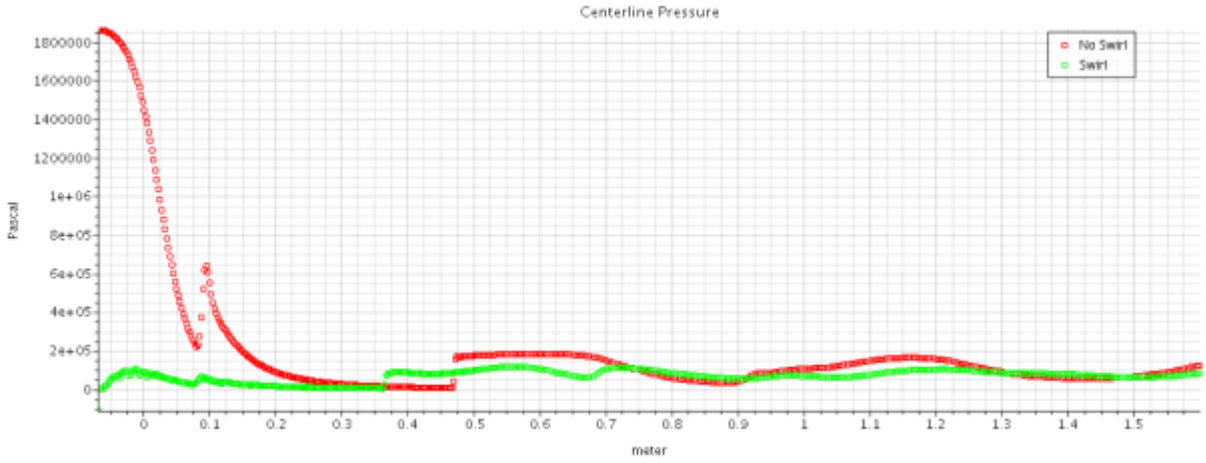

Figure 36. Pressure Along the Symmetry Axis of the Body

The pressure plots in Figures 35 and 36 still show a higher centerline pressure for the non-swirling case upstream of the nozzle as in the case of the conical nozzle simulation. The simulation also shows the dampening of swirl velocity downstream of the nozzle outlet as the pressure difference at the centerline between the two flows becomes insignificantly small as shown in Figure 36.

Figure 36 also shows a higher value of pressure drop at the shock location for non-swirling flow i.e. at 0.46m as compared to the drop in pressure in the case of swirling flow at its shock location 0.37m from the nozzle throat. This result should further be confirmed by the pressure scatter plot in the following Figures.

Pressure Scatter

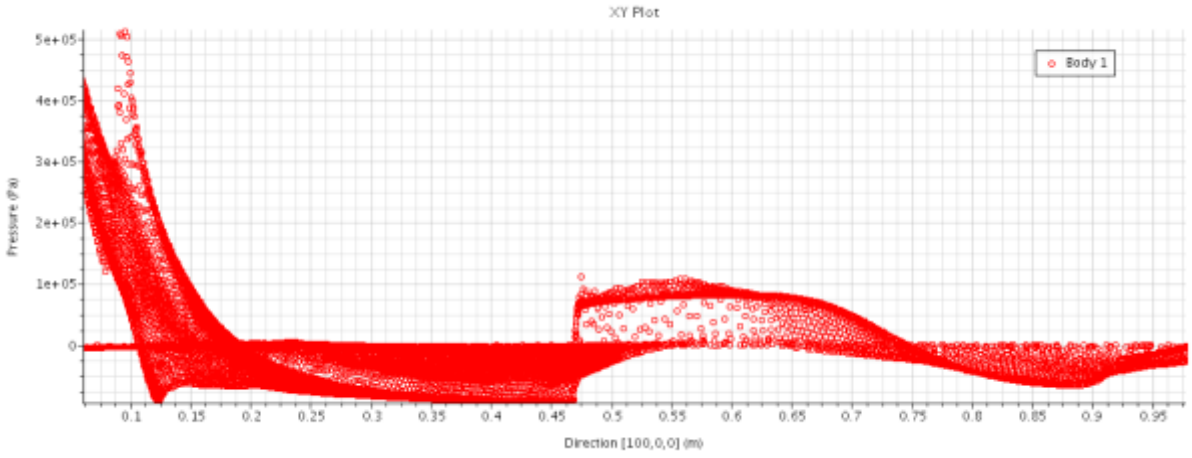

Figure 37. A Scatter Chart for the Various Pressure Values for Non-Swirling Flow

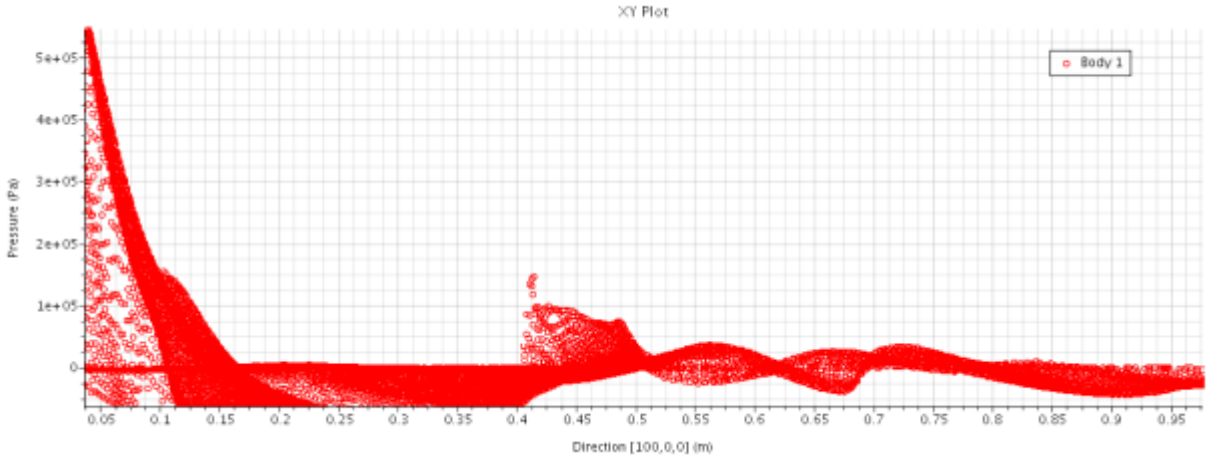

Figure 38. A Scatter Chart for the Various Pressure Values for Swirling Flow

In pressure scatter plots in Figure 37 and Figure 38, the location of the shocks is completely different from what is seen in other figures for the swirling flow case. The scatter plot also shows a higher intensity of shock for the swirling flow case as compared to the non-swirling flow case. This is in contradiction to the results obtained in the conical nozzle case. It is thus possible that the change in location and intensity of the shock from the conical case is caused due to the difference in how the wall expands (linear vs parabolic). The results obtained also deviate from the experimental and theoretical results from Mager and Norton [11] [12]. However, since trumpet-bell nozzles were not used in the experimental and theoretical solutions, the contradiction cannot be evidently concluded.

Density

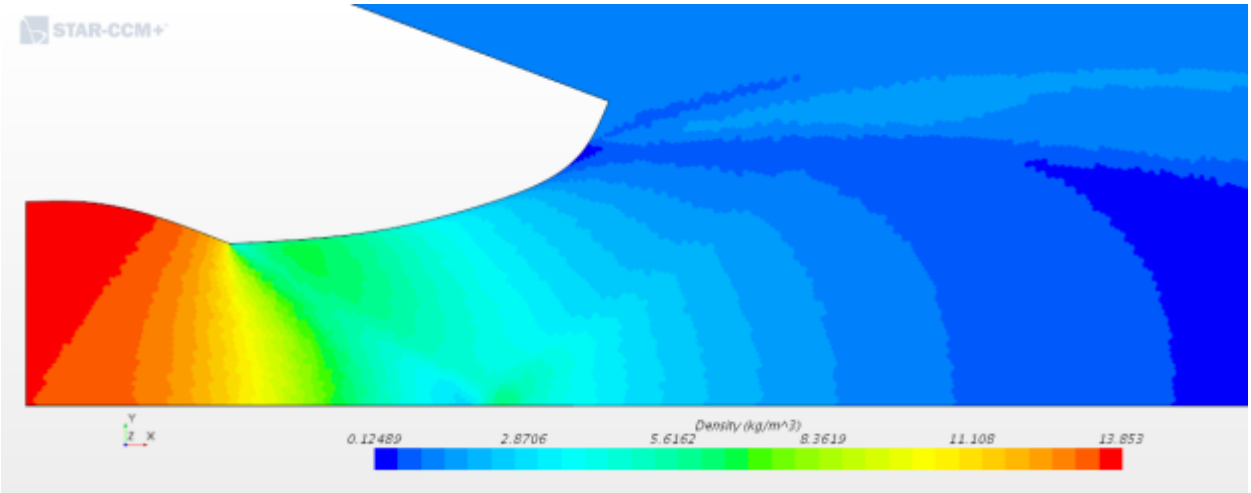

Figure 39. Density Contours of Non-Swirling Fluid

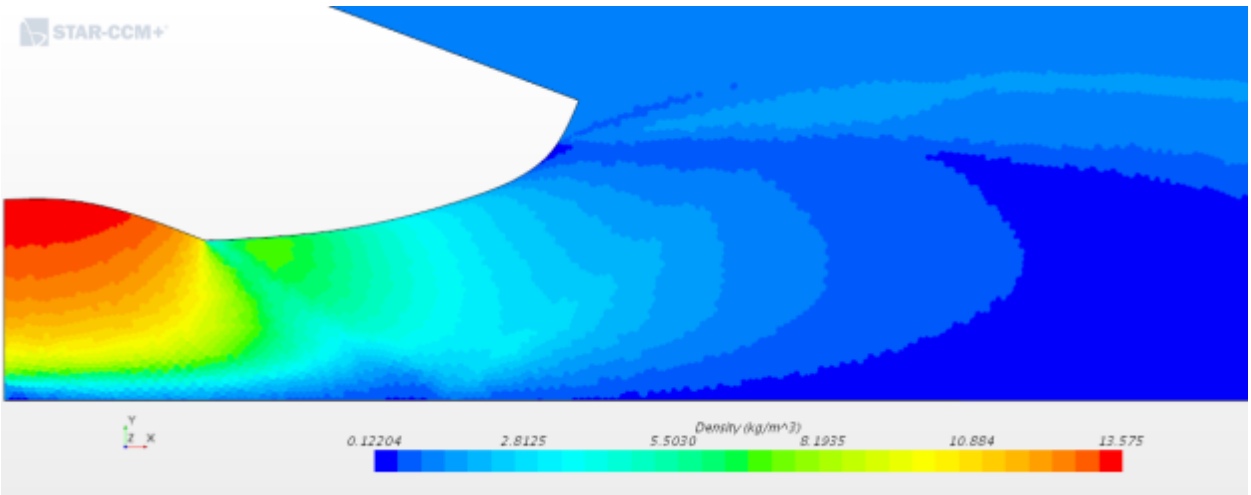

Figure 40. Density Contours of Swirling Fluid

The density values are in accordance with the results in the conical nozzle case with no exceptions. As seen in the conical nozzle case, difference can be seen in the densities at the wall and the centerline in the case of swirling and non-swirling flows. The contours are more vertical in the non-swirling case and tend to get inclined towards the horizontal axis in the swirling case.

This difference is evident closer to the nozzle throat and diminishes as we go father, showing signs of reducing vortex and the flow becoming almost purely axial.

Mass Flow Rate at Outlet

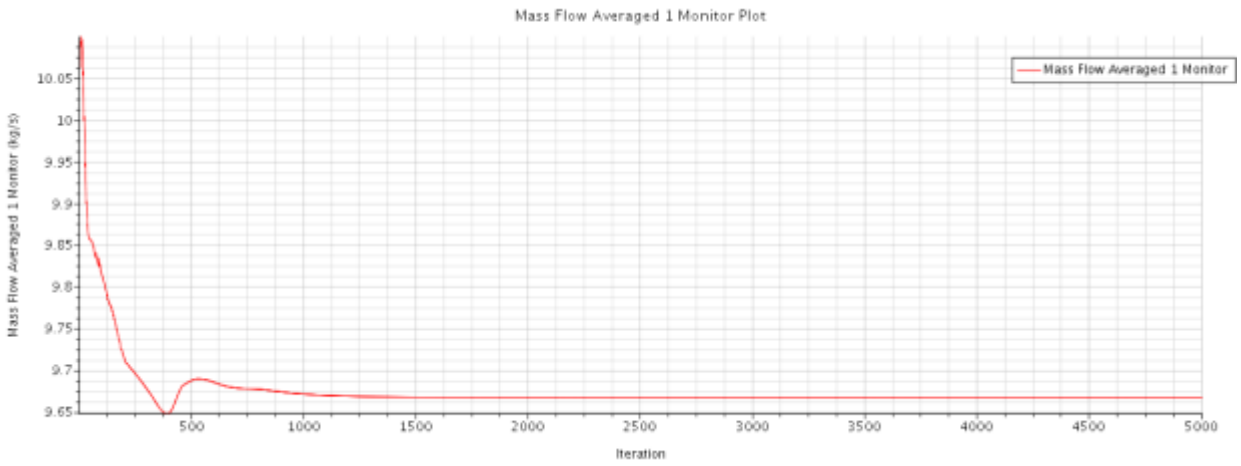

Figure 41. Average Mass Flow Rate at the Outlet for Non-Swirling Fluid

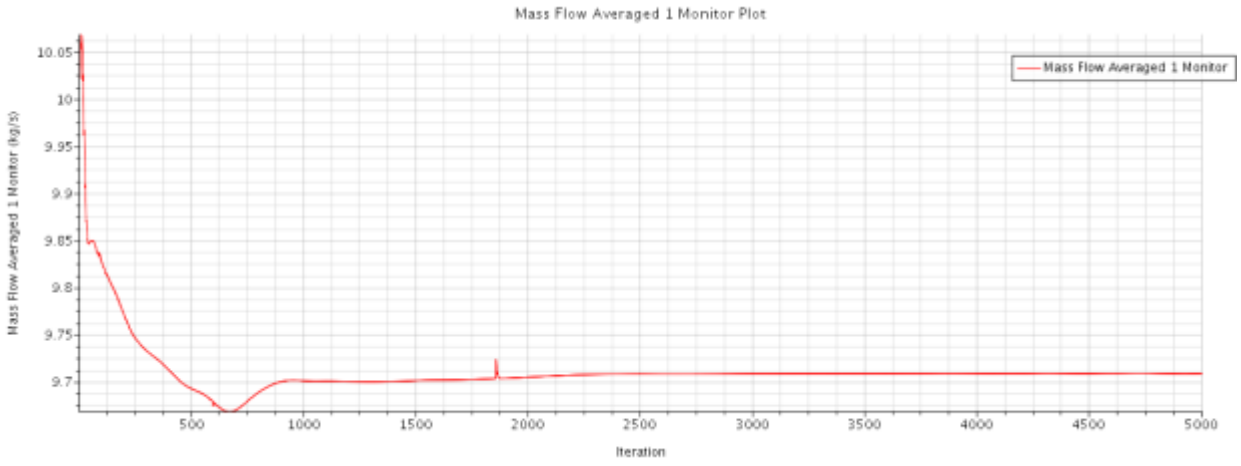

Figure 42. Average Mass Flow Rate at the Outlet for Swirling Fluid

Comparing the mass flow rates shows a higher mass flow rate for the swirling flow as compared to the non-swirling flow, which is not in agreement with results in case of conical nozzle. This can be attributed to the fact that the mass flow rate is measured at the outlet of the system boundary as defined in Figure 8, which is not the same as the outlet of the nozzle. An extended boundary downstream of the nozzle is just created to get a bigger and more accurate picture of the nozzle simulations. Unsuccessful efforts were made to calculate the mass flow rate at the exit boundary of the nozzle due to complications and limitations of the software.

One possible cause of the error in case of the parabolic nozzle was considered to be the sharp edge at the throat of the nozzle in the nozzle geometry. Sharp edges do not work very well with CFD software and tend to give erroneous results. A geometry without the sharp edge was created and simulated, which showed reduced error in residuals. However, very little change was seen in terms of pressure and outlet mass flow values, which are contradicting the values obtained in the conical nozzle case. Thus, a possible conclusion of the research can be that the nozzle flow behaves differently in case of parabolic and conical nozzles. However, further research needs to be done in this regard to prove the hypothesis.

Chapter 5

Conclusion

The research shows that the swirling flow does not change the location of the shock structures even though there is a considerable change in the intensity of the shocks in case of conical nozzles. In the case of trumpet-bell nozzles, it can be seen that there is a change in the location of the shock which is confirmed by the Mach number and pressure displayers of the simulation. Contradicting results are obtained in terms of the intensity of the shock for the parabolic nozzle case where the Mach number contours, Mach number scatter plots and centerline pressure plots show a reduction in the intensity for the swirling flow case while the pressure scatter shows just the opposite. This, as discussed, can be attributed to error in the simulation. There is also a possibility that the flow behaves differently in the case of conical and parabolic nozzles as shown in the simulations. However, further investigation into this discrepancy is required.

There is also a reduction in the mass flow rate at the outlet of the nozzle when a swirling flow is simulated through the nozzle in the conical nozzle case even though the difference didn't appear to be significant. Thus swirling flow can provide better mass flow control at the outlet of the nozzle. This is in agreement with the research conducted by Mager [12] where he used numerical methods to determine the reduction in mass flow rate for a nozzle with swirling flow as compared to one without swirling flow. However, the outlet used in this simulation to measure the mass flow rate is the outlet of the geometry rather than the outlet of the nozzle and the results thus

cannot be considered conclusive. This outlet was used instead of the original nozzle outlet due to the restrictions of the CFD software.

The values used for the simulations were also used to verify the values found by Talamantes [8] shown in appendix 1. The pressure ratios, area ratios and swirl velocities show agreement for both nozzle geometries. Even though conclusive evidence cannot be provided, the conical nozzle is recommended for further projects with the particular bidirectional vortex engine design.

Even though Star CCM+ results can be considered to be reliable more simulations can be run on the nozzle with different working conditions and finer meshes can be used. More research needs to be conducted on the parabolic nozzles to obtain conclusive results. Different input and output conditions can be used with a variety of pressure ratios to get more accurate and conclusive data on the shock structures and the mass flow rates at the outlets of the parabolic nozzle. Lastly, mass flow rate values need to be calculated at the actual outlet of both the nozzles rather than at the boundaries of the extended geometries.

Appendix A

Rocket Combustion Chamber and Nozzle Dimensions

Overall Chamber Dimensions		
	in	mm
Combustion Length	9.5	241.3
Radius	4	101.6
Diameter	8	203.2
Convergence Length	1.5	38.1
Total Length	11	279.4
Aspect Ratio	1.375	
Mantle fraction	0.707	
Combustion Radius	2.828	71.831
Combustion Diameter	5.656	143.662
Combustion Area	25.125	16209.74
Combustion Volume	238.689	3911410.87

Mass Flow (kg/s)		
Total	11.873	
RP-1 Inlet	3.664	31%
LOX Inlet	8.208	69%
Mixture ratio mass	2.24	
Theory	1.59	
Actual	2.118	

Performance	
Outlet Velocity (m/s)	2417.462
Thrust (N)	28701.927
Thrust (Lbf)	6452.451

Nozzle Design

Chamber Pressure (Pa)	2100000		Outlet Pressure (Pa)	101325
	inches	mm		
Throat Radius	2.191	55.640	P_exit/P_chamber	0.048
Throat Diameter	4.381	111.280	Mach #	2.579
Throat Area	15.075	9725.846	Outlet Diameter	8.233
Fillet Opening Diameter	5.656	143.662	Outlet Radius	4.117
Fillet Opening Radius	2.828	71.831	Outlet Area	53.241
			Outlet Area Ratio	3.532
Chamber	3571	3297.850	5968.13	
Throat	3188.393	2915.243	5279.437143	
Outlet	1986.017	1712.867	3115.159923	

REFERENCES

[1]"First Launch", NASA, 2017. [Online]. Available: http://www.nasa.gov/multimedia/imagegallery/image_feature_644.html. [Accessed: 05- Feb- 2017].

[2]"Why did NASA End the Space Shuttle Program?", Gizmodo.com, 2017. [Online]. Available:http://gizmodo.com/why-did-nasa-end-the-space-shuttle-program-1721140493. [Accessed: 05- Feb- 2017].

[3]R. Pielke Jr and R. Byerly, "Shuttle programme lifetime cost", Nature, vol. 472, no. 7341, 2011.

[4] Sverdrup Technology, Inc., "Rocket Combustion Chamber Life- Enhancing Design Concepts", AIAA, Brook Park, Ohio, 1990.

[5] D. Huzel and D. Huang, Design of liquid propellant rocket engines, 1st ed. Washington: Scientific and Technical Information Office, National Aeronautics and Space Administration, 1971.

[6] R. Jewett and J. Halchak, "The Use of Alloy 718 in the Space Shuttle Main Engine", The Minerals, Metals and Materials Society, Canoga Park, CA, 1991.

[7]"Vortex rocket engine", Celestialmechanics.co.uk, 2017. [Online]. Available: http://www.celestialmechanics.co.uk/vortex.html. [Accessed: 03- Feb- 2017].

[8] Gerardo Talamantes and Brian A. Maicke. "Evaluation of CFD Codes for Swirl-Driven Combustors", 46th AIAA Fluid Dynamics Conference, AIAA AVIATION Forum, (AIAA 2016-4393) http://dx.doi.org/10.2514/6.2016-4393

[9]"De Laval nozzle", *En.wikipedia.org*, 2017. [Online]. Available: https://en.wikipedia.org/wiki/De_Laval_nozzle. [Accessed: 03- Mar- 2017].

[10]"Converging Diverging Nozzle", Engapplets.vt.edu, 2017. [Online]. Available: http://www.engapplets.vt.edu/fluids/CDnozzle/cdinfo.html. [Accessed: 03- Mar- 2017].

[11] D. J. Norton, B. W. Farquhar, and J. D. Hoffman. An analytical and experimental investigation of swirling flow in nozzles. AIAA Journal, 7(10):1992_2000, 1969.doi:10.2514/3.5493.

[12] Artur Mager. Approximate solution of isentropic swirling flow through a nozzle. ARSJournal, 31(8):1140_1148, 1961. doi:10.2514/8.5732.

[13] National Aeronautics and Space Association, "Oblique Shock Waves", NASA, 2015.

[14] L. J. Manda. Spin effects on rocket nozzle performance. Journal of Spacecraft andRockets, 3(11):1695_1696, 1966. doi:10.2514/3.28733.

[15] M. Chiaverini, M. Malecki, J. Sauer, W. Knuth, and C. Hall. Vortex combustion Chamber development for future liquid rocket engine applications. In 38thAIAA/ASME/SAE/ASEE Joint Propulsion Conference and Exhibit , 2002.

[16] K. Kitagawa, T. Mitsutani, T. Ro, and S. Yuasa. Effects of swirling liquid oxygen flow on combustion of a hybrid rocket engine. In 40th AIAA/ASME/SAE/ASEE Joint Propulsion Conference and Exhibit, 2004.

[17] D. Papamoschou and A. Johnson, "Unsteady Phenomena in Supersonic Nozzle Flow Separation", American Institute of Aeronautics and Astronautics, University of California, Irvine, Irvine, CA 92697-3975, 2006.

ACADEMIC VITA

Academic Vita of Rohan Gaglani
rmg5491@psu.edu

Education:
Bachelor of Science in Mechanical Engineering
Honors Student of the Schreyer Honors College

Thesis Title:
Simulation of Swirling Flow Through a Nozzle for a Bidirectional Vortex Rocket Engine

Thesis Supervisor:
Dr. Brian Maicke, Associate Professor of Mechanical Engineering

Grants Received:
Hartzler Travel Grant
Penn State Harrisburg Travel Scholarship
Penn State Harrisburg Honors Program Scholarship

Awards:
Penn State Harrisburg Alumni Associations Award.

Professional Memberships:
The Society of Automotive Engineers(SAE)

Community Service Involvement:
Peru Service Learning Trip, Spring 2016

International Education:
Peru Service Learning Trip, Spring 2016.

Language Proficiency: English, Gujarati, Hindi, Marathi